Journal of Hydrology 566 (2018) 23–42

Contents lists available at ScienceDirect

Journal of Hydrology

journal homepage: www.elsevier.com/locate/jhydrol

Research papers

A copula-based analysis of projected climate changes to bivariate flood quantiles

Jiabo Yin[a], Shenglian Guo[a,*], Shaokun He[a], Jiali Guo[b], Xingjun Hong[a], Zhangjun Liu[a]

[a] State Key Laboratory of Water Resources and Hydropower Engineering Science, Wuhan University, Wuhan 430072, China
[b] College of Hydraulic and Environmental Engineering, China Three Gorges University, Yichang 443002, China

ARTICLE INFO

This manuscript was handled by A. Bardossy, Editor-in-Chief, with the assistance of Amir Agha Kouchak, Associate Editor

Keywords:
Climate change
Bivariate analysis
Copula function
Flood frequency analysis
Ganjiang River basin

ABSTRACT

Climate change will lead to great impacts on flood frequency curve and design floods in the future. However, traditional hydrologic approaches often fail to analyze the flood characteristics within a bivariate framework under changing environment. Moreover, previous studies investigating bivariate characteristics of flood usually do not derive the adaptive flood quantiles. This study assesses the implications of climate change for future bivariate quantiles of flood peak and volume in Ganjiang River basin, China. The outputs of two global climate models (BNU-ESM and BCC-CSM1.1) are statistically downscaled by Daily bias correction (DBC) method and used as inputs of the Xinanjiang hydrological model to simulate streamflow during 1966–2099. Projections for future flood (2020–2099) under Representative Concentration Pathway (RCP) 8.5 scenario are divided into two 40-year horizons (2040s, 2080s) and a comparison is made between these time horizons and the baseline (1966–2005). Univariate flood frequency analysis indicates that there is a considerable increase in the magnitude and frequency of flood under the RCP8.5 scenario, especially for the higher return periods. The bivariate quantile curves under different levels of Joint Return Period (JRP) for historical and future periods are derived by copula functions and the most likely realizations are estimated. It is found that climate change has heavier impacts on the future joint bivariate quantiles for larger return periods. Finally the adaptive isolines and most likely flood quantiles under a JRP are derived from analyzing the merged series by non-stationary copula-based models. The results highlight that the joint probability, illustrated by the isoline of a given JRP, varies significantly over time when non-stationary models are applied. This study incorporates the impacts of climate change on bivariate flood quantiles and develops an adaptive quantile estimation approach, which may provide useful information for the references of flood risk assessment and management under changing environment.

1. Introduction

Changes in the climate are presently taking place due to the high greenhouse gas concentrations in the atmosphere. According to the Fifth Assessment Report (AR5) of the Intergovernmental Panel on Climate Change (IPCC, 2014), spatial patterns of projected temperature and precipitation show large increases over land, particularly over high-latitude regions of the Northern hemisphere. Increase in temperature and precipitation can significantly affect flood dynamics, and change to flood characteristics has great impacts on various water resources sectors including flood protection, reservoir management, ecosystem, etc. Hence, it is of great importance to assess characteristics of extreme events such as floods in the context of changing climate to enable appropriate adaptation strategies.

Global Climate Models (GCMs), based on mathematical representations of atmosphere, ice cap, ocean and land surface processes, are considered to be the most comprehensive and dependable tools available to generate information about current and future climate for various greenhouse gases and aerosols concentration scenarios (IPCC, 2014; Swansburg et al., 2004). As ones of the GCMs, the BCC-CSM1.1 developed by Beijing Climate Center in China Meteorological Administration and the BNU-ESM developed by Beijing Normal University in China, have been currently popular used over China due to their good performance in reproducing observed climate variations in China in recent decades. For example, Xin et al. (2013) showed that the BCC-CSM1.1 has good capability in reproducing the time evolutions of mean surface air temperature over China. Ji et al. (2014) demonstrated that the BNU-ESM enables successfully simulating many observed features of the earth climate system in China, such as the climatological annual cycle of surface air temperature and precipitation, annual cycle

* Corresponding author.
E-mail addresses: yj2498@columbia.edu (J. Yin), slguo@whu.edu.cn (S. Guo).

https://doi.org/10.1016/j.jhydrol.2018.08.053
Received 20 June 2017; Received in revised form 1 March 2018; Accepted 24 August 2018
Available online 31 August 2018

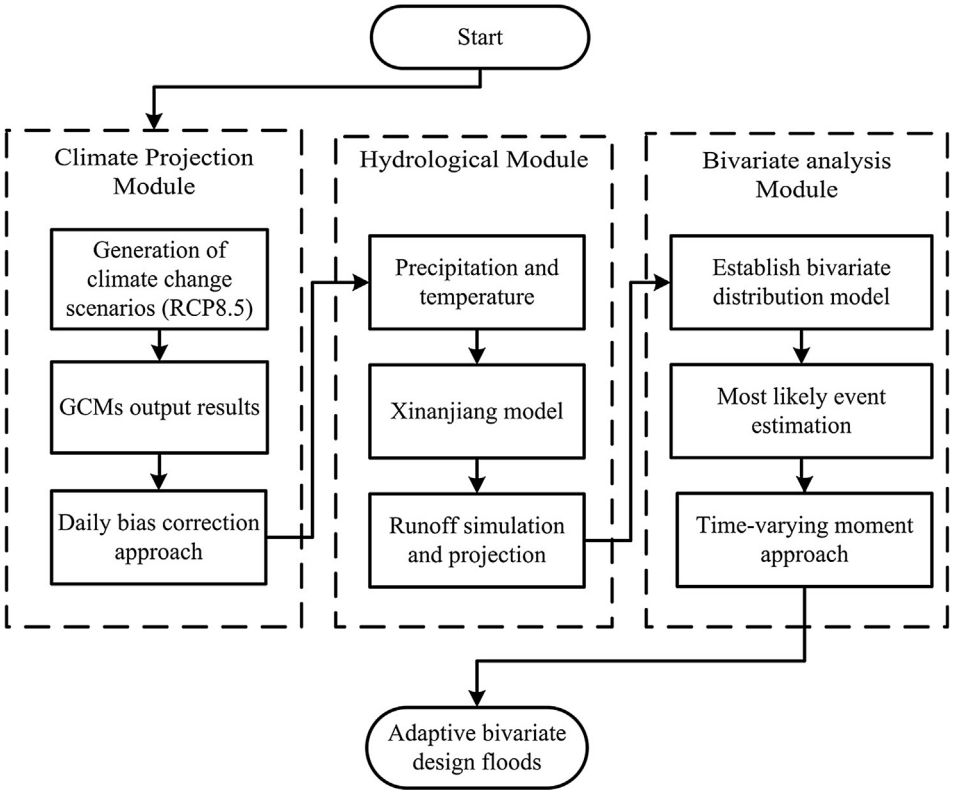

Fig. 1. Flowchart of adaptive flood quantile estimation procedure.

of tropical pacific sea surface temperature, etc. Wang et al. (2016) verified that the BCC-CSM1.1 associating with statistical downscaling simulates the precipitation and temperature well in the Ganjiang River basin. Ma et al. (2016) employed the BNU-ESM to reproduce the precipitation and temperature in historical period and verified its good performance in the Xiangjiang River basin.

The assessment of climate impacts at the local to regional scale usually requires the use of downscaling methods to translate large-scale GCM outputs to regionally more-relevant scales (Chen et al., 2011). The downscaling methods contain statistical downscaling and dynamic downscaling (i.e. regional climate models, RCMs) techniques (Durman et al., 2001; Themeßl et al., 2010). Previous studies have proved that the statistical downscaling methods have advantages of inexpensive computation efficiency over dynamic downscaling (e.g. Xu, 1999; Wilby et al., 2002; Mpelasoka and Chiew, 2009; Chen et al., 2013a,b; Shen et al., 2018). For the statistical downscaling approaches, the bias correction methods are widely used for the ease of implementation and relatively good performance (Themeßl et al., 2010; Teng et al., 2012; Ahmadalipour et al., 2018; Zhuan et al., 2018). Chen et al. (2013a) proposed a Daily bias correction (DBC) approach, which is a hybrid method combing the Local intensity scaling method (Schmidli et al., 2006) and the Daily translation method (Mpelasoka and Chiew, 2009) to correct both the wet day frequency and the distribution of wet day precipitation. Several authors have successfully employed the DBC method to correct the GCM raw outputs and verified its good performance (e.g. Chen et al., 2013b; Zhang et al., 2017; Shen et al., 2018; Zhuan et al., 2018).

Over the past decade a limited number of studies focusing on the projected changes to flood characteristics have been conducted, and most of these are within a univariate flood frequency analysis framework (e.g. Prudhomme et al., 2002; Booij, 2005; Das et al., 2011; Huziy et al., 2013; Tofiq and Guven, 2014, 2015; Meaurio et al., 2017). The univariate frequency analysis is unable to describe the probability of occurrence for the flood event, which is generally characterized by multivariate variables such as flood peak and volumes (e.g. Shiau, 2003; Yin et al., 2018). Therefore, multivariate flood frequency analysis is essential for better understanding of projected changes to flood characteristics. Until now, only a very few studies address the multivariate characteristics of flood events under changing climate. For example, Jeong et al. (2014) evaluated climate change impacts on three spring flood characteristics, i.e. flood peak, volume and duration, within a bivariate framework, for 21 northeast Canadian basins covering Québec and some parts of the adjoining Ontario and Newfoundland provinces of Canada. Duan et al. (2016) explored the variations of flood frequency in the Huai River basin under different climate change scenarios by fitting univariate distribution as well as copula function. The influence of the expected changes on multivariate flood frequency curve and joint design floods will significantly affect dam safety in the future, and the adaptive flood quantiles will provide rich information as the references for flood risk assessment and is essential for future water resources design and management. However, how to derive the adaptive flood quantiles under changing environment has been rarely investigated.

The aim of the paper is to investigate the impacts of climate change on flood quantiles of flood peak and volume within a bivariate framework and to derive adaptive bivariate flood quantiles by non-stationary copula approaches for the Ganjiang River basin in China. The remainder of the paper is organized as follows. Section 2 is devoted to Copulas and bivariate analysis method. Section 3 introduces observed and simulated data and their processing in the Ganjiang River basin. In section 4, the application of the adaptive flood quantile estimation procedure is analyzed and discussed. At last, the paper ends with the conclusions.

2. Methodology

The flowchart of adaptive flood quantile estimation procedure is given in Fig. 1, on which there are three modules. The climate projection module generates the future climate conditions by two GCMs (BCC-CSM1.1 and BNU-ESM) and the precipitation and temperature

data are statistically downscaled into basin scale. The hydrological module simulates and projects future flow discharge using the Xinanjiang hydrological model. The bivariate analysis module compares the projections between the future and historical floods within bivariate framework and then derives the projected isolines and most likely flood quantiles under non-stationary models by time-varying moment method.

2.1. General copulas and bivariate return period

This study focuses on flood peak and volume to investigate the joint probability of flood occurrence. The Copula function, a promising mathematical tool proposed by Nelsen (1999, 2006), is found versatile for constructing joint distribution functions as it allows modeling the dependence structure among random variables independently of the marginal distributions (Salvadori and De Michele, 2004; Favre et al., 2004). Every joint distribution can be written in terms of a copula and its univariate marginal distributions. Let $F_{xi}(xi)$ $(i = 1,2,\ldots,n)$ be the marginal cumulative density functions (CDFs) of X_i. The multivariate probability distribution H is expressed in terms of its marginal distributions and the associated dependence function, known as Sklar's theorem (Sklar, 1959):

$$C_\theta(F_{X_1}(x_1), F_{X_2}(x_2), \ldots, F_{X_n}(x_n)) = H_{X_1,X_2,\ldots,X_n}(x_1, x_2, \ldots, x_n) \quad (1)$$

where C, called copula, is uniquely determined whenever $F_{xi}(xi)$ are continuous, and captures the essential features of the dependence among the random variables; θ is the parameter of copula.

In the conventional univariate analysis, flood events of interest are often defined by return periods. In the bivariate domain; however, it is still discussed by the community which method is most suitable to transform the joint exceedance probability to a bivariate Joint Return Period (JRP). Different JRPs estimated by copula functions have been developed for the case of a bivariate flood frequency analysis. Eight types of possible joint events were presented by Salvadori and De Michele (2004) using "OR" and "AND" operators, in which, two cases are of the greatest interest in hydrological applications (Shiau, 2003; Salvadori and De Michele, 2004; Yin et al., 2017, 2018):

(1) (OR case) either $Q > q$, or $W > w$, i.e.

$$E_{\text{or}} = \{Q > q \text{ or } W > w\} \quad (2)$$

(2) (AND case) both $Q > q$ and $W > w$, i.e.

$$E_{\text{and}} = \{Q > q \text{ and } W > w\} \quad (3)$$

In simple words: for E_{or} to happen it is sufficient that either flood peak discharge (Q) or flood volume (W) or both exceed given thresholds; instead, for E_{and} to happen it is necessary that both Q and W are larger than prescribed values. Hence, two different JRPs can be defined accordingly (De Michele et al., 2005):

$$T_{or} = \frac{\mu}{P[Q > q or W > w]} = \frac{\mu}{1-F(q, w)} \quad (4)$$

$$T_{and} = \frac{\mu}{P[Q > q and W > w]} = \frac{\mu}{1-F_Q(q)-F_W(w) + F(q, w)} \quad (5)$$

where μ is the mean inter-arrival time between two consecutive events, and $F(q, w) = P(Q \leqslant q,\ W \leqslant w)$.

Moreover, different definitions of the multivariate return period are available in literature, based on regression analysis, bivariate conditional distributions, survival Kendall distribution function and structure performance function. A comprehensive review of the JRP estimation methods was given by De Michele et al. (2013), Volpi and Fiori (2014) and Salvadori et al. (2016), and references therein. In this study, the bivariate phenomenon being studied for Q and W is defined based on Eq. (4) in the case of annual maxima $\mu = 1$ year.

2.2. Parametric and nonparametric estimation methods

Prior to conduct the bivariate analysis, it is necessary to find the best-fit marginal and joint distribution functions. Hence, a set of parametric and nonparametric estimation methods are evaluated in this study.

2.2.1. Parametric estimation methods

In this study, five widely used parametric distributions, i.e. Lognormal, Gamma, Gumbel, Generalized extreme value (GEV) and Pearson type III (P-III), are used for fitting Q and W series. The parameters of marginal distribution functions are estimated using L-moments (LM) method (Hosking, 1990). The first four orders of LMs can be defined by probability-weighted moments (PWMs) as:

$$\begin{aligned} \lambda_1 &= \beta_0, \\ \lambda_2 &= 2\beta_1 - \beta_0, \\ \lambda_3 &= 6\beta_2 - 6\beta_1 + \beta_0, \\ \lambda_4 &= 20\beta_3 - 30\beta_2 + 12\beta_1 - \beta_0. \end{aligned} \quad (6)$$

in which, β_r denotes the PWMs defined as (Greenwood et al., 1979):

$$\beta_r = \int_0^1 x(F)F^r dF \quad (7)$$

Different families of Copula functions have been proposed and described by Nelsen (2006). The Archimedean family is an associative class of copulas, which allows modeling dependence in arbitrarily high dimensions with only one parameter (Nelsen, 2006). The Archimedean family is more desirable for hydrological analyses because it can be easily constructed and applied to whether the correlation among the hydrological variables is positive or negative (Yin et al., 2017). Three one-parameter Archimedean copulas, including the Gumbel-Hougaard (G-H), Frank and Clayton copulas, have been applied in flood frequency analysis by many authors (e.g. Shiau, 2003; Zhang and Singh, 2006; Requena et al., 2016), and thus are selected as the candidates in modeling the bivariate dependence between Q and W. For estimating the copula parameter θ, the most common used method is the Kendall correlation coefficient (Bender et al., 2014; Xu et al., 2016) and is adopted in this study.

2.2.2. Nonparametric estimation method

For the parametric estimation methods, the flood data series are assumed to be drawn from a known distribution. However, the probability distribution is never known in practice (Guo and Kachroo, 1996; Poulin et al., 2007). The nonparametric estimation method, which does not require the assumption of any distribution, is used and compared with the parametric estimation methods.

The marginal probability density function (PDF) for Q and W series is estimated using a nonparametric kernel density method that incorporates a weighted moving average of the empirical frequency distribution (Scott, 1992). Given a set of observations, $x_1, \ldots, x_n$, a univariate kernel density estimator is expressed as

$$\hat{f}(x) = \frac{1}{nh}\sum_{i=1}^{n} K\left(\frac{x-x_i}{h}\right) \quad (8)$$

where $K(\bullet)$ is the kernel function, n is the number of observations and h is the bandwidth that controls the variance of the kernel function. The choice of the bandwidth h is an important issue in estimating the PDF because the kernel estimator is highly sensitive to bandwidth (Adamowski, 1985; Guo and Kachroo, 1996; Vittal et al., 2015). To asymptotically optimize h, an overall measure of the effectiveness of $\hat{f}(x)$ is provided by minimizing the mean integrated squared error (MISE), which is given as follow (Bowman and Azzalini, 1997):

$$\text{MISE} = E\left[\int \{\hat{f}(x) - f(x)\}^2 dx\right] \approx \frac{1}{4}h^4\alpha_k^4 \int f''(x)^2 dx + \frac{1}{nh}\alpha \quad (9)$$

Table 1
Archimedean copula functions with time dependent parameter θ_c^t and time dependent generator function $\varphi(p, t)$.

Copula function	Copula expression $C_{\theta_c^t}$	Generator ϕ(p, t)	Range of *PleaseCheck*
Gumbel-Hougaard	$\exp\{-[(-\ln u)^{\theta_c^t} + (-\ln v)^{\theta_c^t}]^{1/\theta_c^t}\}$	$(-\ln p)^{\theta_c^t}$	$(1, \infty)$
Clayton	$[u^{-\theta_c^t} + v^{-\theta_c^t} - 1]^{-1/\theta_c^t}$	$\frac{p^{-\theta_c^t} - 1}{\theta}$	$(0, \infty)$
Frank	$-\frac{1}{\theta_c^t}\ln[1 + \frac{(e^{-\theta_c^t u} - 1)(e^{-\theta_c^t v} - 1)}{e^{-\theta_c^t} - 1}]$	$-\ln(\frac{e^{-\theta_c^t p} - 1}{e^{-\theta_c^t} - 1})$	$R\backslash\{0\}$

where $p = u$ or $p = v$.

where $\alpha = \int K^2(x)dx$ and α_k^2 denotes the variance of kernel function $\int x^2 K(x)dx$.

The bivariate kernel density estimator can be established in a manner similar to that of the univariate kernel. A product of the univariate kernel functions is used to expand the kernel density estimators to the bivariate distributions with a set of bandwidths (h_x, h_y). The joint distribution is estimated as (Silverman, 1986; Vittal et al., 2015):

$$f(x, y) = \frac{1}{nh_x h_y}\sum_{i=1}^{n}\{K(\frac{x-x_i}{h_x})K(\frac{y-y_i}{h_y})\} \tag{10}$$

where (x_i, y_i) are the bivariate observations; h_x, h_y are the bandwidths in the x and y directions, respectively. The MISE for the bivariate kernel case is expressed as follows (Silverman, 1986):

$$\mathrm{MISE} = \frac{1}{4}h^4\alpha^2\iint\{\nabla^2 f(x, y)\}^2 dxdy + \frac{1}{nh^2\beta} \tag{11}$$

where $\alpha = \int xyK(x, y)dxdy$, $\beta = \int K(x, y)^2 dxdy$ and ∇^2 is the Laplace operator. The optimal bandwidth for a bivariate kernel is also obtained by minimizing the MISE.

In this study, the Gaussian distribution is selected as the kernel function since it has been widely employed in fitting flood series and demonstrates good performance (e.g. Adamowski, 1985; Silverman, 1986; Vittal et al., 2015). The optimal bandwidth is obtained following the general form proposed by Bowman and Azzalini (1997).

2.3. Non-stationary extreme value theory

In a bivariate framework, non-stationarity can emerge in the statistical attributes of the univariate variables and/or in the dependence structure of the variables. To capture the possible non-stationary property of the marginal distributions, the adaptive flood quantiles are derived by employing time or meteorological variables as covariates in the non-stationary framework and incorporating the statistical downscaling of future meteorological covariates from GCMs. The non-stationary flood series are evaluated using the time-varying moment method, which is built under the Generalized Additive Models in Location, Scale and Shape (GAMLSS) framework (Rigby and Stasinopoulos, 2005).

For the time-varying moment of three-parameter distributions $f_X(x^t|\mu_t, \sigma_t, \kappa_t)$ at time t ($t = 1, 2, ..., n$), both the location parameter μ_t, scale parameter σ_t and shape parameter κ_t can be expressed as a linear or non-linear function of the explanatory variables E_j^t ($j = 1, 2, ..., m$) through the monotonic link functions given by

$$\begin{aligned} g(\mu_t) &= \alpha_{10} + \textstyle\sum_{j=1}^{m}\alpha_{1j}E_j^t \\ g(\sigma_t) &= \alpha_{20} + \textstyle\sum_{j=1}^{m}\alpha_{2j}E_j^t \\ g(\nu_t) &= \alpha_{30} + \textstyle\sum_{j=1}^{m}\alpha_{3j}E_j^t \end{aligned} \tag{12}$$

where $g(\cdot)$ is the monotonic link function, which is determined by the domain of the statistical parameterθ_X, i.e. if $\theta_X \in R$, $g(\theta_X) = \theta_X$ (R indicates real set) or if $\theta_X > 0$, $g(\theta_X) = \ln(\theta_X)$; m is number of explanatory variables; E_j^t indicates the j^{th} explanatory variables at time t and α_{ij} ($i = 1, 2, 3$, $j = 0, 1, ...m$) are the GAMLSS parameters.

2.4. Non-stationary copula functions

To model temporal changes of the dependence between hydrological variables, the copula parameter θ is substituted by the time dependent copula parameter θ_c^t as shown in Table 1.

Similar to a univariate distribution, the parameters of a copula are assumed to be functions of an explanatory variable (time or meteorological variables) to define a non-stationary copula. Based on the definition of a copula, the non-stationary bivariate copula of flood peak and volume can be described as following:

$$F^t(q^t, w^t) = C[F_Q^t(q|\theta_Q^t), F_W^t(w|\theta_W^t)|\theta_c^t] \tag{13}$$

where $F^t(q^t, w^t)$ indicates the time-varying joint distribution of Q and W series; $F_Q^t(\cdot)$, $F_W^t(\cdot)$ and θ_Q^t, θ_W^t represents the time-varying CDFs and parameters for Q and W data series, respectively.

Similarly, those parameters of a non-stationary copula are expressed as the following linear function of the explanatory variables:

$$g_c(\theta_c^t) = \beta_0 + \sum_{j=1}^{m}\beta_j E_j^t \tag{14}$$

where $g_c(\cdot)$ is a link function of the copula, if $\theta_c^t \in R$ (for Frank copula), $g_c(\theta_c^t) = \theta_c^t$ or if $\theta_c^t > 0$ (for G-H and Clayton copulas), $g_c(\theta_c^t) = \ln(\theta_c^t)$; $\beta_0, \beta_1, ..., \beta_m$ are the GAMLSS parameters. The parameters of the time-varying marginal and joint distributions are estimated by the IMF method proposed by Joe (2005).

2.5. Non-stationary most likely event selection on isoline

The critical level curve shown in Fig. 2 is defined as bivariate quantile curve under the OR JRP. The function that describes the level curve for any given JRP T_{or} or critical probability level p has two asymptotes, $q = q_p$ and $w = w_p$, where $q_p = F_Q^{-1}(p)$ and $w_p = F_W^{-1}(p)$ are the marginal distribution quantiles for a given probability level p. According to Eq. (4) in the bivariate case, the choice of an appropriate JRP

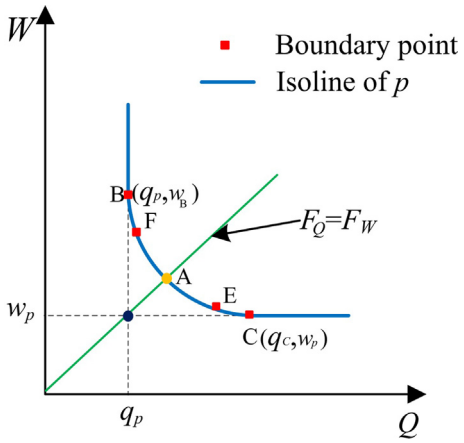

Fig. 2. Bivariate quantile curve (isoline) and feasible region with a critical probability level p.

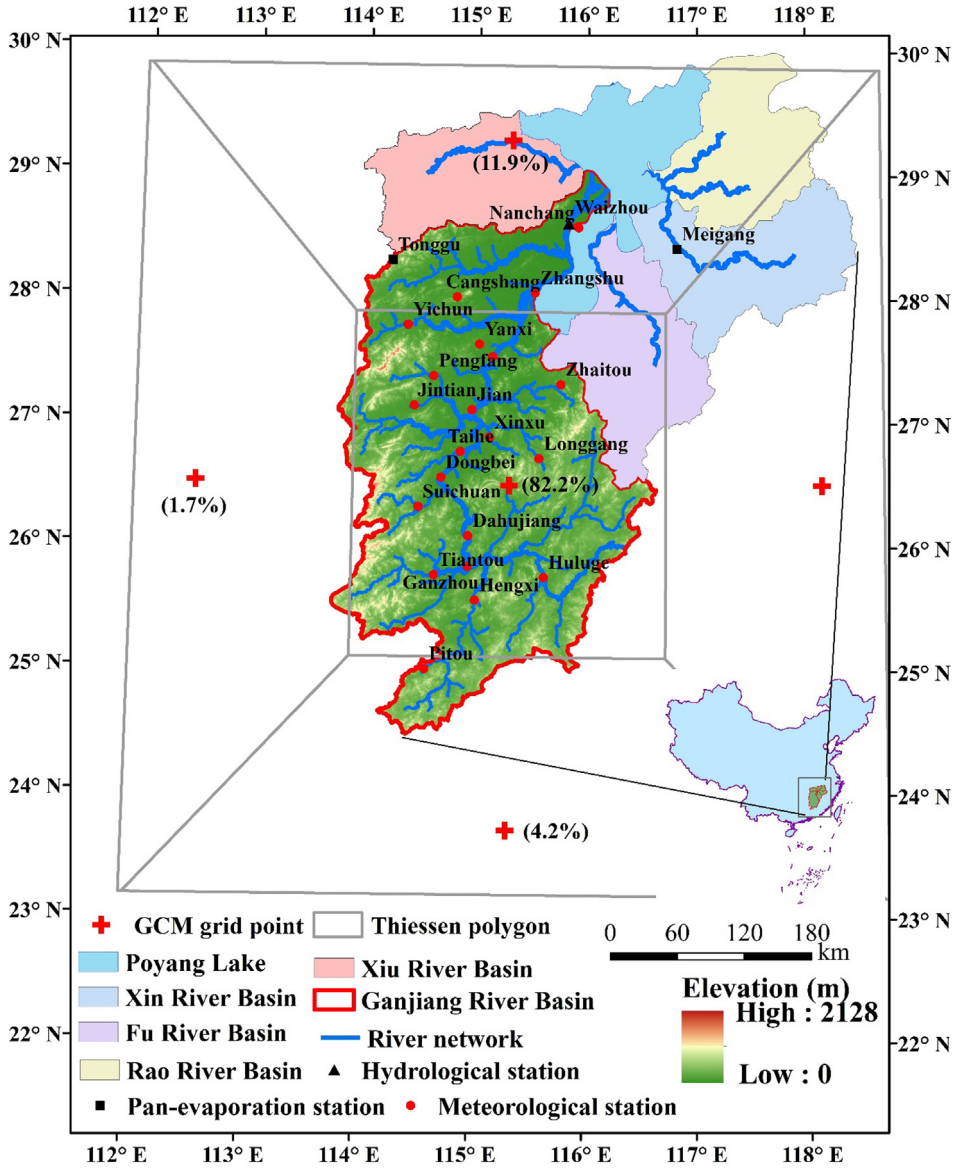

Fig. 3. Meteorological, pan-evaporation and hydrological stations and GCMs grid points used in this study.

T_{or} will lead to infinite combinations of Q and W in the isoline. Even though all points on a p-level curve have the same joint probability, the different likelihood of each point must be taken into account to select appropriate design scenarios (Salvadori et al., 2011). Chebana and Ouarda (2011) segmented the p-level curve into a central part (i.e. the subset EF in Fig. 2) and a tail part by employing its geometric properties. Salvadori et al. (2011) proposed the novel concept of "most likely design realization" to choose the point with the highest likelihood along the p-level curve. Volpi and Fiori (2012) defined the distance of each point along the quantile curve from its vertex as random variable and derive its PDF, then derived the confidence interval of the conditional distribution as well as the "central part". Despite the fact that the advancement of "central part" contributes to explore the inherent law of hydrology, unique design quantiles under one certain standard are necessary for engineering practice. Xu et al. (2016) proposed the conditional most likely combination (CMLC) method and conditional expectation combination (CEC) method to describe the dependence between flood peak and volumes by using the conditional density function to measure the occurrence likelihood of flood events, in which the CMLC and CEC methods are only suitable for univariate conditional return period.

In this study, the most likely design realization method proposed by Salvadori et al. (2011) is applied in the non-stationary data series and derived as follows:

(1) The non-stationary joint distribution function $F^t(q^t, w^t)$ is expressed in terms of its marginal functions $F_Q^t(q)$ and $F_W^t(w)$ by using an associated non-stationary copula function C, i.e. $F^t(q, w) = C_{\theta^t}(u, v)$, and $u = F_Q^t(q)$, $v = F_W^t(w)$.

(2) For a given JRP, the corresponding p-level curve can be obtained by solving Eq. (13), and then the most likely flood event $[q^*(t), w^*(t)]$ of all possible events at this level is derived by selecting the point with the largest joint probability density:

$$\begin{cases} [q^*(t), w^*(t)] = \arg\max\ f_t(q, w) = c_{\theta^t}[F_Q^t(q), F_W^t(w)] \cdot f_{Q_t}(q) \cdot f_{W_t}(w) \\ C_{\theta^t}[F_Q^t(q), F_W^t(w)] = 1 - 1/T_{or}, \quad t = 1, 2, \ldots, n \end{cases} \tag{15}$$

where $f_t(q, w)$ is a non-stationary joint PDF of q and w; $c_{\theta^t} = dC_{\theta^t}(u, v)/dudv$ is the density function of copula for non-stationary data series; $f_{Q_t}(q)$ and $f_{W_t}(w)$ are the PDF of $F_Q^t(q)$ and $F_W^t(w)$, respectively.

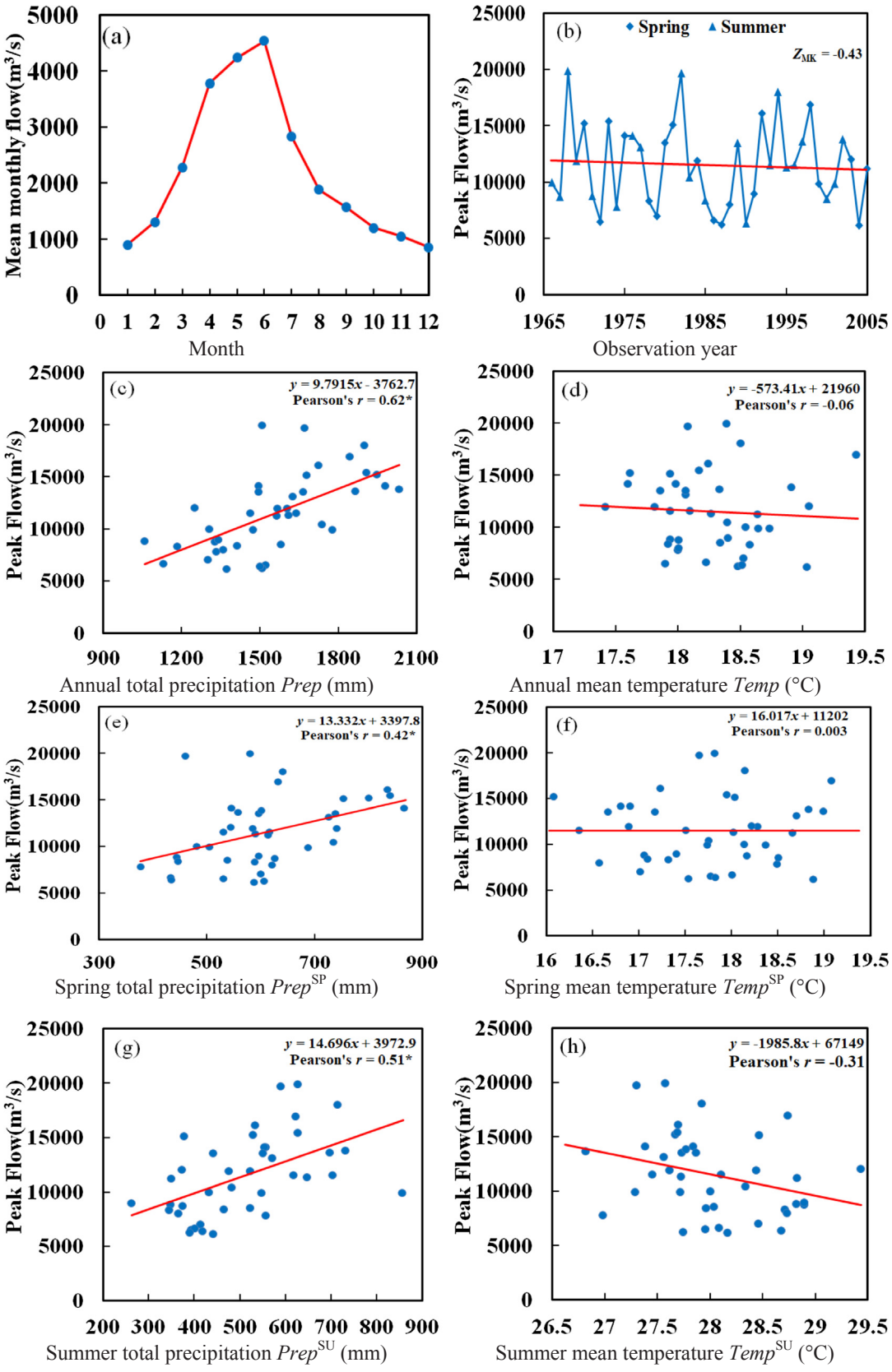

Fig. 4. Monthly average streamflow and regression plots between the observed peak discharge series at Waizhou station and basin average meteorological data in Ganjiang River basin (*indicates significant at 5% significance level).

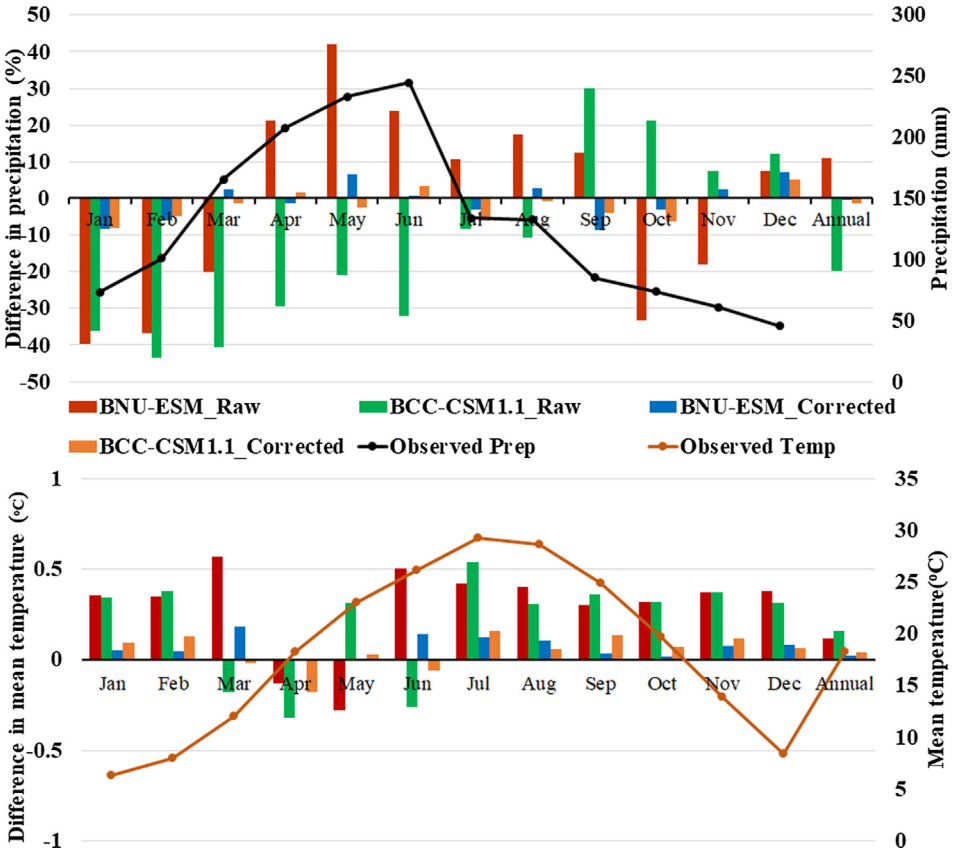

Fig. 5. Differences between observed basin average meteorological variables and climate baselines (1966–2005) before and after bias correction at monthly and annual scales in Ganjiang River basin.

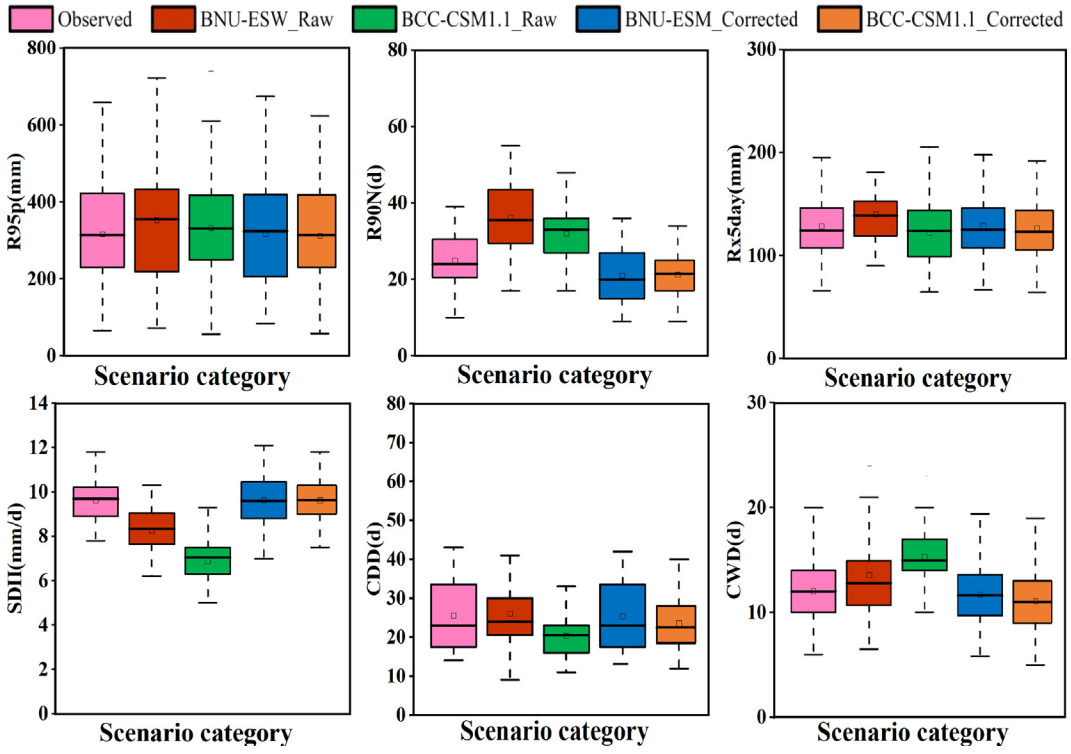

Fig. 6. Comparison of observed and simulated EPIs using historical BNU-ESM and BCC-CSM1.1 outputs during 1966–2005 before and after bias correction.

(3) The Lagrange multiplier method (Chen and Singh, 2018) is applied for solving Eq. (15) to obtain the most likely realization along the level curve.

For a given JRP T_{or}, the Lagrange function is constructed as below:

$$\varphi_t(q, w) = c_{\theta^t}[F_Q^t(q), F_W^t(w)]f_{Q_t}(q)f_{W_t}(w) + \lambda_t\{C_{\theta^t}[F_Q^t(q), F_W^t(w)]-(1-1/T_{or})\} \quad (16)$$

where λ_t is the Lagrange multiplier at time t.

(4) The first order derivative equals to zero will reach the maximum value and the following equation should be satisfied

$$\begin{cases} \varphi_{q_t} = f_{W_t}(w)[c_u^t f_{Q_t}^2(q) + c_{\theta^t}(u, v)f'_{Q_t}(q)] + \lambda_t \frac{\partial C_{\theta^t}[F_Q^t(q), F_W^t(w)]}{\partial u} f_Q^t(q) = 0 \\ \varphi_{w_t} = f_{Q_t}(q)[c_v^t f_{W_t}^2(w) + c_{\theta^t}(u, v)f'_{W_t}(w)] + \lambda_t \frac{\partial C_{\theta^t}[F_Q^t(q), F_W^t(w)]}{\partial v} f_W^t(w) = 0 \\ \varphi_{\lambda_t} = C_{\theta^t}[F_Q^t(q), F_W^t(w)]-(1-1/T_{or}) = 0 \end{cases} \quad (17)$$

where $c_u^t = \partial c_{\theta^t}(u, v)/\partial u$, $c_v^t = \partial c_{\theta^t}(u, v)/\partial v$; $f'_{Q_t}(q)$ and $f'_{W_t}(w)$ is the derivative function of $f_{Qt}(q)$ and $f_{Wt}(w)$, respectively.

The nonlinear Eq. (17) can be solved by numerical methods, such as the harmonic mean Newton's method (Özban, 2004).

3. Case study

3.1. Basin

The Ganjiang River basin shown in Fig. 3, a tributary basin of the Yangtze River is located between 24.48°–29.07° N and 113.67°–116.65° E, central-south China with a total area of 80948 km^2 and total length of 766 km. The river originates in southwestern Jiangxi province and runs into the southern plains, finally falling into the Yangtze River. The Ganjiang River is the largest river among the five that flow into Poyang Lake, and the other four rivers are Fu, Xin, Rao and Xiu Rivers. Poyang Lake is the largest fresh water lake in China, and the water from the Poyang Lake flows through the outlet to Yangtze River in the north. The five rivers are all within the Poyang Lake watershed. As the water level in the Poyang Lake is influenced by the five rivers as well as the Yangtze River, the seasonal variation of water level and discharge create a unique landscape of fresh water lake-wetland ecosystem. The Poyang Lake wetland is among one of the major habitats of global importance for wintering migratory birds (Hu et al., 2007). Hence, the Ganjiang River located in the southern part of Poyang Lake watershed, it plays a vital role in supplying water to support Poyang Lake's ecological environment. This basin spans four latitudes, and the natural head of mainstream reaches 937 m.a.s.l., which results in inhomogeneous spatial and temporal distribution of precipitation. The mean annual precipitation in the whole Ganjiang River basin is 1540 mm, while the mean annual precipitation in middle Ganjiang River basin is 1413 mm. Due to such distribution characteristics of precipitation, heavy rainstorms rarely occurred in the Jian-Taihe basin and southern Ganjiang River in the recent 50 years. The basin has a typical subtropical humid monsoon climate, and the mean annual temperature is 17.8 °C. The highest and lowest temperatures are 39.5 °C and −5.8 °C, respectively.

3.2. Data

Observed daily precipitation and temperature data of 11 meteorological stations in the Ganjiang River basin from 1966 to 2005 were obtained from China Meteorological Data Sharing Service System (http://cdc.cma.gov.cn/index.jsp), and these stations are evenly distributed over the Ganjiang River basin as shown in Fig. 3. In addition, observed daily pan-evaporation data at Nanchang, Tonggu and Meigang stations and flow discharge data at Waizhou station during 1966–2005 were collected from the Hydrology and Water Resources Bureau of Jiangxi Province, China. Waizhou hydrological station is the outlet of Ganjiang River basin, whose discharge represents the properties of the characteristics of hydrological regime.

Fig. 4a shows that the runoff is concentrated during spring (March, April and May) and summer (June, July and August) seasons at the Waizhou station. The annual maximum peak discharge (Q) trend during 1966–2005 is extracted and drawn in Fig. 4b, and non-significant decreasing trend is detected by the Mann-Kendall test (Mann, 1945; Ma et al., 2016) with the statistic $Z_{MK} = -0.43$, compared to the critical value of$Z_{1-\alpha/2} = -1.96$ at the $\alpha = 5\%$ significance level. Only a few low-intensity snowfalls occurred during 1966–2005 and they all happened in winter, so the impact of snowmelt on summer floods is neglect in the Ganjiang River basin. Temperature and precipitation are two meteorological variables that are closely related to streamflow and are chosen as potential covariates for investigating the climate-flood relationship. The basin average meteorological series are obtained by aggregating the observed data of different stations over the watershed using Thiessen polygon method. Then the annual total precipitation and annual average temperature series (denoted by *Prep* and *Temp*, respectively) over the period of 1966–2005 are extracted. Fig. 4c–d reveal that Q has much higher dependence on *Prep* than *Temp*, and the correlation between Q and *Prep* is significant at 5% significance level. Considering all the observed floods occurred in spring and summer (see Fig. 4b), total precipitation and average temperature during these two seasons (denoted by $Prep^{SP}$, $Temp^{SP}$ and $Prep^{SU}$, $Temp^{SU}$, respectively) are also examined. Regression plots between the observed flood series

Table 2
Estimated parameters of Xinanjiang model in Ganjiang River basin.

Number	Parameter	Explanation	Value	Unit
1	KE	Ratio of potential evapotranspiration to pan evaporation	0.842	/
2	WM	Areal mean tension water storage capacity	168.774	mm
3	UM	Upper layer tension water storage capacity	18.207	mm
4	LM	lower layer tension water storage capacity	75.052	mm
5	B	Tension water distribution index	0.239	/
6	IMP	Impermeable coefficient	0.039	/
7	SM	Areal mean free water storage capacity	44.543	mm
8	EX	Free water distribution index	1.406	/
9	KI	Out flow coefficient of free water storage to interflow	0.144	/
10	KG	Out flow coefficient of free water storage to groundwater flow	0.121	/
11	C	Deep layer evapotranspiration coefficient	0.162	/
12	CI	Interflow recession coefficient	0.480	/
13	CG	Groundwater recession coefficient	0.965	/
14	n	Parameter of Nash unit hydrograph	1.526	/
15	NK	Parameter of Nash unit hydrograph	2.649	/

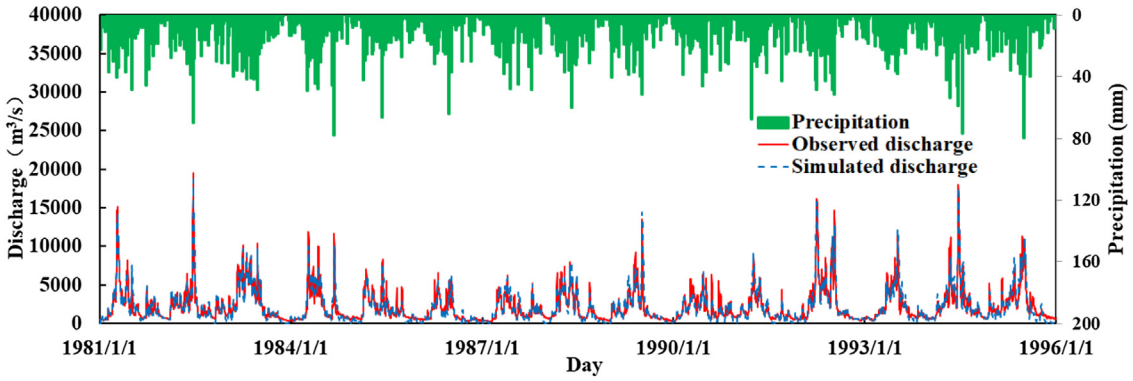

(a) Daily discharge during part of calibration period (1981-1995)

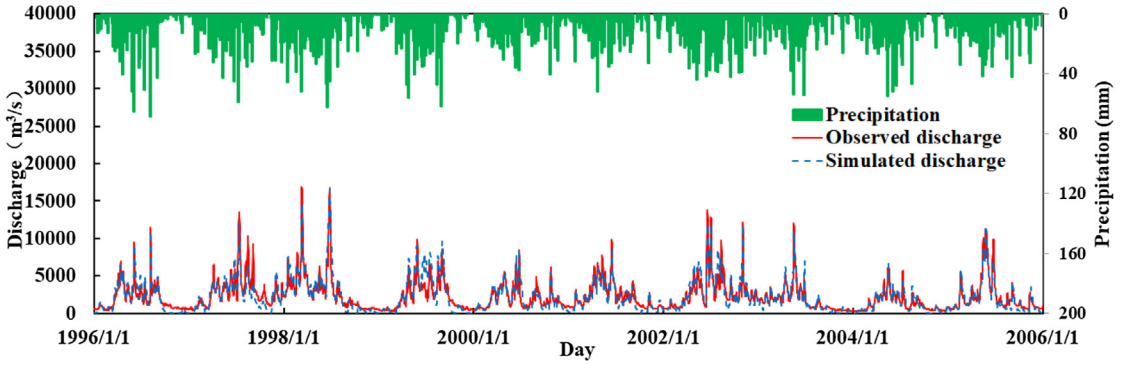

(b) Daily discharge during verification period (1996-2005)

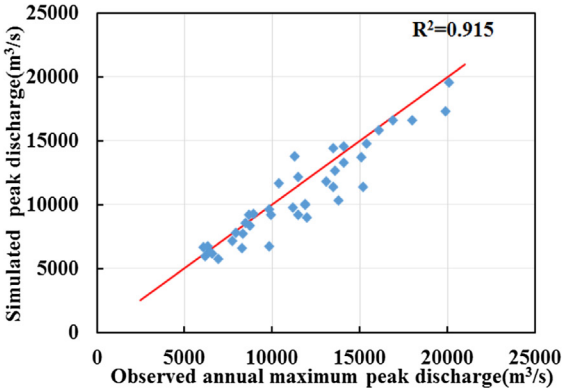

(c) Annual maximum peak discharge during 1966-2005

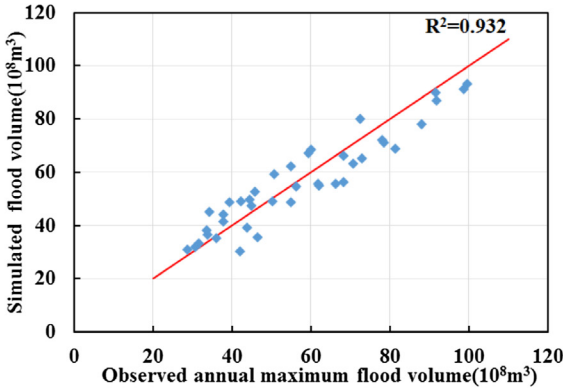

(d) Annual maximum 7-day flood volume during 1966-2005

Fig. 7. Comparison of simulated and observed daily discharge (a–b), simulated and observed annual maximum values (c–d) at Waizhou station in the Ganjiang River basin.

and seasonal meteorological variables (Fig. 4e–h) indicate that seasonal statistics have lower correlation coefficients comparing with annual statistics except that the $Temp^{SU}$ has stronger relation than *Temp*. Overall, the Pearson correlation coefficient between *Q* and *Prep* with the value of 0.62 significantly overweigh the other five variables.

The climate model simulations were taken from the database of phase 5 of the Coupled Model Intercomparison Project 5 (CMIP5) database. Two GCMs, i.e. the BCC-CSM1.1 and the BNU-ESM, under Representative Concentration Pathway (RCP) 8.5 scenario were selected in this study. These two GCMs have the same horizontal resolution (2.8° lat. ×2.8° long.), and four grid points were chosen to include all areas with noticeable influence on the circulation patterns that govern climate in the Ganjiang River basin. The precipitation and temperature data from GCM simulations are aggregated over the watershed to obtain the basin average series using the Thiessen polygon method. Fig. 3 also presents the Thiessen polygon derived from the

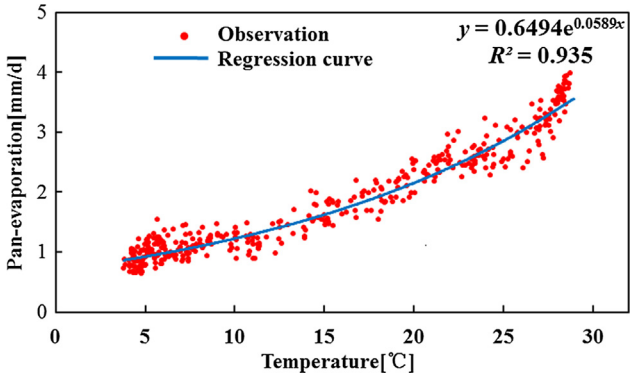

Fig. 8. Regression analysis results between the observed mean annual daily pan-evaporation and temperature in the Ganjiang River basin.

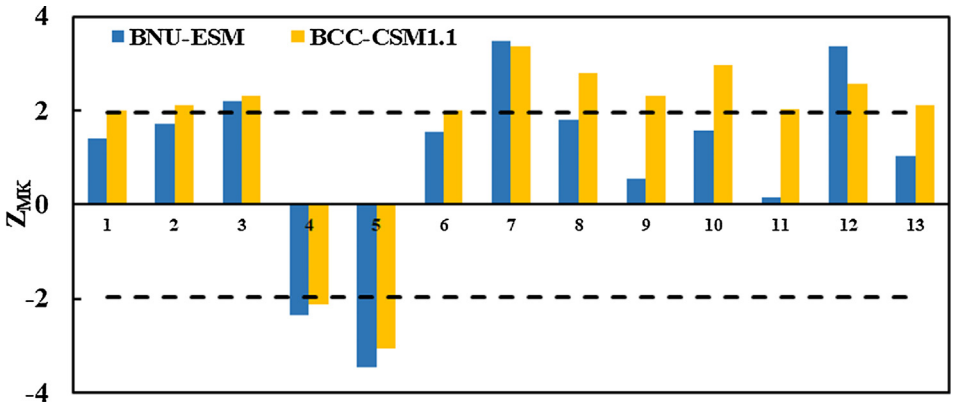

Fig. 9. Mann-Kendall trend test statistic Z_{MK} of climate variables and EPIs during 1966–2099 in the Ganjiang River basin.

GCM grid points, and the representative ratio of each grid point is also denoted. The outputs of the BCC-CSM1.1 and BNU-ESM GCMs consist of daily precipitation and temperature during 1966–2099. The future periods (2020–2099) are divided into two parts: near-future (2020–2059, 2040s) and far-future (2060–2099, 2080s), while the simulations of historical period (1966–2005) of the two GCMs are served as a reference for future projection and change.

3.3. Statistical downscaling of GCM outputs

As introduced above, GCM outputs are too coarse to directly drive a hydrological model for impact studies, and so the downscaling technique must be utilized. In this study, an empirical statistical downscaling method, i.e. Daily bias correction (DBC) approach proposed by Chen et al. (2013a,b) is applied to deal with the systematic errors of GCMs raw basin average precipitation and temperature data.

The DBC is a hybrid method combining the daily translation (DT) and local intensity scaling (LOCI) methods. The LOCI method is first employed to correct the precipitation occurrence. For a particular month (e.g. January) in the reference period, a wet-day threshold is determined from the GCM to ensure that the threshold exceedance equals the observed wet-day frequency for that month. The threshold is applied to the future period to correct the GCM's precipitation in corresponding month. The DT method is then employed to correct the frequency distributions of precipitation amounts and temperatures. This DBC method takes advantage of the LOCI method to correct precipitation occurrence. Instead of applying the same factor to each daily precipitation (e.g. the LOCI method) for a specific month, it modulates the change as a function of the daily precipitation amount (or temperature) based on quantile differences in the frequency distribution of precipitation (or temperature) for the observed data.

To implement the DT method, a distribution mapping technique is used to establish a relationship between the observed precipitation $P_{obs,Q}$ or temperature $T_{obs,Q}$ (at different percentiles) and the GCM-simulated data ($P_{GCM,ref,Q}$, $T_{GCM,ref,Q}$) for a specific month at the reference period. The ratios of precipitation and temperature between observed and GCM-simulated data at the reference period are calculated for each percentile. The adjusted daily precipitation $P_{adj,fut,d}$ for the future period can be obtained by multipling the percentile ratio, and the adjusted daily temperature $T_{adj,fut,d}$ for the future period can be derived by adding

Table 3
Projected future changes of annual mean precipitation, temperature, discharge and EPIs under two GCMs.

ID	Variable	BNU-ESM			BCC-CSM1.1		
		Historical	2040s	2080s	Historical	2040s	2080s
1	Annual discharge (m^3/s)	2128.1	2113.2	2172.5	2108.2	2158.2	2205.3
	Variation (%)	/	−1.2	2.1	/	2.4	4.6
2	Spring discharge (m^3/s)	3449.4	3515.0	3539.6	3410.1	3578.6	3618.8
	Variation (%)	/	1.9	2.6	/	4.9	6.1
3	Summer discharge (m^3/s)	3257.1	3324.0	3358.0	3243.2	3378.2	3411.8
	Variation (%)	/	2.1	3.1	/	4.2	5.2
4	Autumn discharge (m^3/s)	941.9	856.0	829.2	932.6	878.5	752.3
	Variation (%)	/	−9.1	−12.0	/	−5.8	−8.6
5	Winter discharge (m^3/s)	747.9	561.0	515.8	825.7	696.7	594.7
	Variation (%)	/	−25.6	−31.0	/	−15.6	−28.0
6	Prep(mm)	1536.0	1542.2	1599.8	1531.0	1593.1	1623.0
	Variation (%)	/	0.4	4.2	/	4.1	6.0
7	Temp (°C)	18.3	20.3	22.7	18.3	20.3	22.2
	Variation (%)	/	10.8	23.9	/	10.8	21.0
8	R95p (mm)	317.7	306.9	350.2	312.9	336.2	413.8
	Variation (%)	/	−3.4	10.2	/	7.5	32.3
9	R90N (d)	21.5	20.9	23.1	20.7	22.7	24.6
	Variation (%)	/	−2.8	7.4	/	9.7	18.8
10	Rx5day (mm)	129.2	127.5	137.9	126.4	135.1	148.2
	Variation (%)	/	−1.3	6.7	/	6.9	17.3
11	SDII (mm/d)	9.6	9.6	9.8	9.5	9.9	10.4
	Variation (%)	/	−0.9	1.7	/	4.2	9.5
12	CDD (d)	23.7	26.4	31.4	22.6	25.7	27.5
	Variation (%)	/	11.4	32.7	/	13.7	22.0
13	CWD (d)	12.7	12.1	14.6	12.3	13.6	14.9
	Variation (%)	/	−4.8	14.7	/	10.6	21.1

Table 4
Performance of the parametric and nonparametric methods in fitting Q and W under two GCMs.

	Distribution	Peak			Volume		
		RMSE	AIC	D_{ks}	RMSE	AIC	D_{ks}
Historical							
BNU-ESM	Lognormal	0.042	−249.2	0.089	0.046	−243.1	0.084
	Gama	0.046	−243.2	0.095	0.047	−239.9	0.087
	GEV	0.045	−241.2	0.105	0.048	−236.3	0.089
	Gumbel	0.077	−201.2	0.134	0.077	−201.3	0.105
	P-III	**0.039**	**−253.2**	**0.068**	**0.043**	**−246.6**	**0.075**
	Nonparametric	0.074	−208.5	0.078	0.089	−193.5	0.136
BCC-CSM1.1	Lognormal	0.045	−245.4	0.092	0.044	−246.6	0.097
	Gama	0.044	−245.8	0.089	0.045	−243.8	0.098
	GEV	0.046	−241.2	0.087	0.046	−241.1	0.102
	Gumbel	0.059	−222.5	0.098	0.065	−214.4	0.116
	P-III	**0.040**	**−250.9**	**0.078**	**0.041**	**−249.5**	**0.085**
	Nonparametric	0.049	−240.6	0.089	0.051	−238.3	0.103
2040s							
BNU-ESM	Lognormal	0.134	−156.7	0.112	0.138	−154.5	0.108
	Gama	0.114	−169.9	0.106	0.117	−167.6	0.105
	GEV	0.081	−194.9	0.092	0.088	−188.4	0.095
	Gumbel	0.058	−223.6	0.082	0.068	−211.1	0.092
	P-III	**0.055**	**−225.9**	**0.078**	**0.060**	**−219.1**	**0.081**
	Nonparametric	0.061	−224.2	0.081	0.065	−218.7	0.086
BCC-CSM1.1	Lognormal	0.093	−186.2	0.121	0.105	−176.3	0.124
	Gama	0.081	−197.6	0.124	0.091	−187.4	0.126
	GEV	0.086	−190.4	0.098	0.095	−182.4	0.108
	Gumbel	0.138	−154.6	0.115	0.121	−164.9	0.115
	P-III	0.093	−183.8	0.124	0.099	−179.1	0.105
	Nonparametric	**0.048**	**−243.3**	**0.072**	**0.050**	**−239.1**	**0.075**
2080s							
BNU-ESM	Lognormal	0.103	−177.5	0.098	0.104	−177.4	0.102
	Gama	0.079	−199.5	0.078	0.080	−198.0	0.087
	GEV	0.079	−197.1	0.097	0.083	−193.5	0.092
	Gumbel	0.132	−157.9	0.102	0.115	−169.1	0.115
	P-III	**0.067**	**−210.1**	**0.068**	**0.069**	**−208.1**	**0.075**
	Nonparametric	0.156	−148.6	0.105	0.170	−141.8	0.125
BCC-CSM1.1	Lognormal	0.058	−223.4	0.081	0.065	−214.6	0.083
	Gama	**0.055**	**−227.6**	**0.079**	**0.057**	**−224.7**	**0.078**
	GEV	0.058	−221.9	0.082	0.060	−218.5	0.095
	Gumbel	0.136	−155.6	0.097	0.131	−158.6	0.124
	P-III	0.096	−181.8	0.096	0.058	−221.8	0.082
	Nonparametric	0.096	−187.5	0.095	0.097	−186.3	0.105

D_{ks} smaller than $D_{0,.05} = 0.21$ indicates that the distribution model passes the goodness-of-fit test at 0.05 significance level.

the percentile ratio as following (Chen et al., 2013a; Shen et al., 2018):

$$P_{adj,fut,d} = P_{GCM,fut,d} \times (P_{obs,Q}/P_{GCM,ref,Q}) \quad (18)$$

$$T_{adj,fut,d} = T_{GCM,fut,d} + (T_{obs,Q} - T_{GCM,ref,Q}) \quad (19)$$

where the subscript Q refers to a percentile for a specific month, and the subscript d refers to a specific day in the future period.

The observed basin average meteorological data of the Ganjiang River watershed during 1966–2005 are used as a baseline to correct each GCM. The DBC method calibrated in the reference period is then used to correct the bias of precipitation and temperature for future periods. To evaluate the performance of DBC method, Fig. 5 presents the monthly and annual differences between each baseline projection and observed data for precipitation and mean temperature under two GCMs. The raw projections are denoted as BNU-ESM_Raw and BCC-CSM1.1_Raw respectively, while the GCM simulations after employing the DBC method are denoted as BNU-ESM_Corrected and BCC-CSM1.1_Corrected respectively. Fig. 5 indicates that the two GCMs before bias correction both tend to simulate temperature (maximum difference is 0.54 °C) better than precipitation (maximum difference is 42%) at annual and monthly scale. Since extreme climate events potentially also have impacts on floods than average values, six Extreme precipitation indices (EPIs) including magnitude (R95p and R90N), intensity (Rx5day and SDII) and persistence (CDD and CWD) are selected to assess the capacity of DBC method to simulate the characteristics of extreme precipitation. More interpretations about the EPIs can be found in Wang et al. (2016). The values of EPIs are presented as box plots in Fig. 6, which shows the median (cross), mean (square), 25th and 75th percentiles (box), and 5th and 95th percentiles (whisker).

Fig. 6 reveals that the simulated EPIs corrected by DBC method are significantly closer to those of the observed values. The largest differences of monthly temperature for two GCMs are 0.19 °C, and the difference of monthly precipitation ranges from -8.6% ~ 7.3%. Hence, the DBC method can correct the bias of GCM outputs successfully and use to project future precipitations and temperatures.

3.4. Runoff simulation and projection

Zhao et al. (1980) proposed the Xinanjiang hydrological model and verified the model by using long-term hydrological and climatological data all over China. The Xinanjiang model is a lumped hydrological model, and the main characteristic of this model is the theory of runoff formation on repletion of storage, which means that runoff is not generated until the soil moisture content reaches field capacity. The Xinanjiang model has been widely and successfully applied in the humid and semi-humid climate regions (Zhao, 1992; Lin et al., 2014). The model inputs are the basin average precipitation and pan-

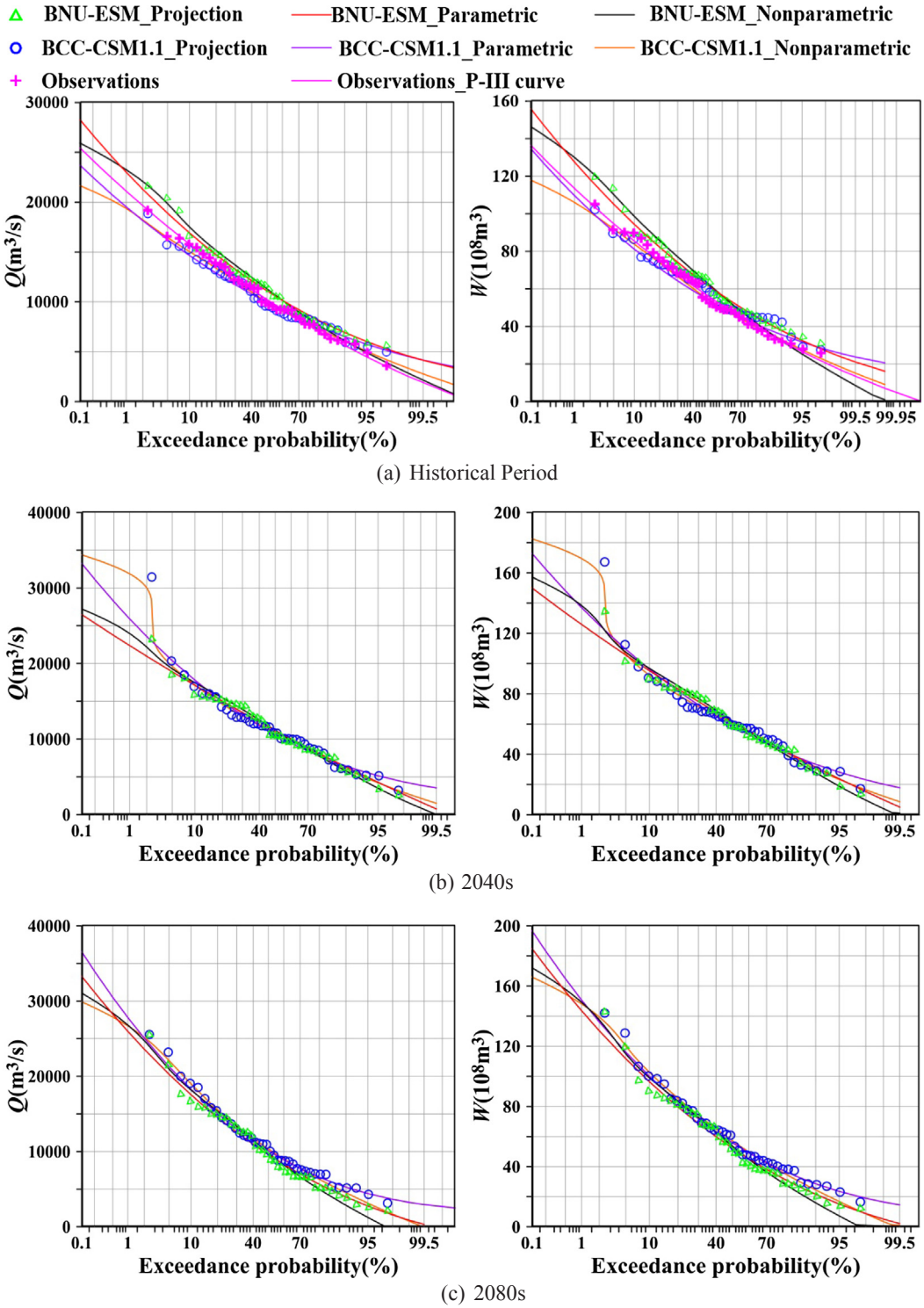

Fig. 10. Probability curves of flood peak discharges and flood volumes under historical and future periods.

Table 5
Correlation coefficient between annual maximum *Q* and *W*.

Correlation coefficient	Observation	BNU-ESM			BCC-CSM1.1		
		Historical	2040s	2080s	Historical	2040s	2080s
Pearson	0.996	0.994	0.995	0.997	0.996	0.993	0.997
Kendall	0.954	0.951	0.956	0.972	0.956	0.938	0.974
Spearman	0.974	0.970	0.971	0.976	0.973	0.971	0.975

Observation indicates the Xinanjiang model simulations using observed meteorological data.

Table 6
Estimated parameters of Copula functions and statistical test results.

Estimation period	Distribution	BNU-ESM				BCC-CSM1.1			
		θ	RMSE	AIC	D_{ks}	θ	RMSE	AIC	D_{ks}
Historical	G-H Copula	**20.53**	**0.007**	**−391.6**	**0.016**	**22.94**	**0.010**	**−370.4**	**0.014**
	Clayton Copula	39.05	0.009	−374.3	0.020	43.88	0.011	−361.1	0.038
	Frank Copula	60.23	0.042	−251.6	0.067	71.09	0.041	−253.0	0.061
	Nonparametric	/	0.011	−360.8	0.023	/	0.013	−347.4	0.036
2040s	G-H Copula	**22.94**	**0.006**	**−410.7**	**0.014**	**16.25**	**0.008**	**−386.9**	**0.018**
	Clayton Copula	43.88	0.007	−394.5	0.024	30.50	0.010	−366.2	0.020
	Frank Copula	71.09	0.026	−290.0	0.039	54.31	0.032	−273.4	0.052
	Nonparametric	/	0.008	−386.3	0.031	/	0.010	−368.4	0.024
2080s	G-H Copula	**35.45**	**0.004**	**−442.5**	**0.007**	**39.00**	**0.003**	**−454.9**	**0.007**
	Clayton Copula	68.91	0.005	−427.8	0.009	75.99	0.004	−434.6	0.008
	Frank Copula	79.15	0.039	−257.5	0.058	83.34	0.043	−249.7	0.068
	Nonparametric	/	0.009	-376.8	0.012	/	0.007	-396.9	0.012

evaporation, and the model outputs include the actual evapotranspiration and flow discharge at the outlet of the basin. In this study, daily hydrological and meteorological data series from 1966 to 1995 and 1996–2005 were used for calibration and verification, respectively. The Rosenbrock method (Rosenbrock, 1960) was used to optimize the parameter values. The estimated parameters of Xinanjiang model and their explanations are listed in Table 2.The mean values of the Nash-Sutcliffe efficiency (NSE) coefficient and Relative Error (RE) are 87.68% and 85.32%; 4.26% and 5.86% during calibration and validation periods, respectively. The observed and simulated discharge hydrographs as well as the annual maximum flood peak and 7-day volume are shown in Fig. 7. Results demonstrate that the Xinanjiang model is able to simulate discharge and reproduce flood events with high NSE, low RE values and high determination coefficient R^2.

The BCC-CSM1.1 and BNU-ESM outputs under RCP8.5 scenario with bias correction were employed to simulate the daily precipitation and temperature during 1966–2099, and then used as the inputs of the calibrated Xinanjiang model to project future flow discharge. Since the future pan-evaporation data cannot be directly measured, it is usually calculated using evaporation estimation methods based on climatic data, varying from simple empirical formulations to complex physically-based methods (Taylor, 2012). In this study, the temperature-based methods suggested in practice (Xu and Singh, 2001; Wang et al., 2016) are employed. The daily average pan-evaporation $EP(t)$ is an approximately exponential function of daily average air temperature $T(t)$, which is given by Wang et al. (2016).

$$EP(t) = A \times \exp(B \times T(t)) \tag{20}$$

where A and B are coefficients determined by the least square method. The regression analysis results between the observed mean annual daily pan-evaporation and temperature during 1966–2005 in the Ganjiang River basin are shown in Fig. 8. The values of determination coefficient R^2 is over 0.93, which indicates that Eq. (20) is reasonable for estimating daily evaporation in this region. Therefore, the pan-evaporation can be estimated by downscaled temperature through the regression Eq. (20) and then used as inputs of Xinanjiang model.

Table 7
Comparison of univariate flood quantiles changes between historical and future periods (Unit: Q, m^3/s; W, $10^8 m^3$).

Estimation period	GCM	Variable	Return Period (year)					
			100	75	50	20	10	5
Observation		*Q*	22878(22657)	22272(22272)	21393(21679)	19282(20037)	17521(18374)	15529(16223)
		W	118.9(111.9)	115.1(109.9)	109.5(106.9)	96.3(98.6)	85.5(89.9)	73.7(78.1)
Historical	BNU-ESM	*Q*	23002(23253)	22302(22800)	21293(22077)	18892(19851)	16918(17517)	14724(15162)
		W	127.6(129.9)	123.8(127.2)	118.3(122.8)	105.2(110.3)	94.3(98.6)	82.2(85.7)
	BCC-CSM1.1	*Q*	19526(19366)	18967(18931)	18161(18236)	16239(16460)	14654(15051)	12886(13374)
		W	109.7(106.0)	106.4(104.0)	101.6(100.7)	90.4(92.0)	81.1(83.8)	71.0(73.9)
2040s	BNU-ESM	*Q*	22390(23985)	21818(23310)	20979(22185)	18910(19311)	17119(17456)	15009(15458)
		Variation(%)	-2.7(3.1)	-2.2(2.2)	-1.5(0.5)	0.1(-2.7)	1.2(-0.3)	1.9(2.0)
		W	125.9(138.4)	122.6(134.5)	117.7(126.7)	105.6(107.6)	95.3(96.8)	83.2(85.4)
		Variation (%)	-1.3(6.5)	-1.0(5.7)	-0.5(3.2)	0.4(-2.4)	1.1(-1.8)	1.2(-0.4)
	BCC-CSM1.1	*Q*	25929(31879)	24973(31100)	23602(29920)	20386(19649)	17797(17144)	14991(14602)
		Variation (%)	32.8(64.6)	31.7(64.3)	30.0(64.1)	25.5(19.4)	21.4(13.9)	16.3(9.2)
		W	137.0(169.5)	132.3(166.1)	125.5(159.7)	109.4(106.4)	96.3(92.4)	82.0(79.4)
		Variation (%)	24.9(59.9)	24.3(59.7)	23.5(58.6)	21.0(15.7)	18.7(10.3)	15.5(7.4)
2080s	BNU-ESM	*Q*	25969(26812)	24997(26002)	23598(24716)	20274(20960)	17551(18178)	14758(15346)
		Variation (%)	12.9(15.3)	12.1(14.0)	10.8(12.0)	7.3(5.6)	3.7(3.8)	0.2(1.2)
		W	143.6(149.3)	138.2(145.3)	130.3(137.5)	111.7(115.0)	96.5(99.1)	82.5(85.9)
		Variation (%)	12.5(14.9)	11.6(14.2)	10.1(12.0)	6.2(4.3)	2.3(0.5)	0.4(0.3)
	BCC-CSM1.1	*Q*	27807(26697)	26674(26060)	23652(24100)	21281(22096)	18273(19013)	15051(15552)
		Variation (%)	42.4(37.9)	40.6(37.7)	30.2(32.2)	31.0(34.2)	24.7(26.3)	16.8(16.3)
		W	150.7(148.2)	144.8(145.0)	129.8(130.4)	116.1(120.3)	100.1(102.7)	82.8(85.5)
		Variation (%)	37.4(39.8)	36.1(39.4)	27.8(29.5)	28.4(30.8)	23.4(22.6)	16.6(15.7)

Values shown in parenthesis () are flood quantiles estimated by nonparametric method.

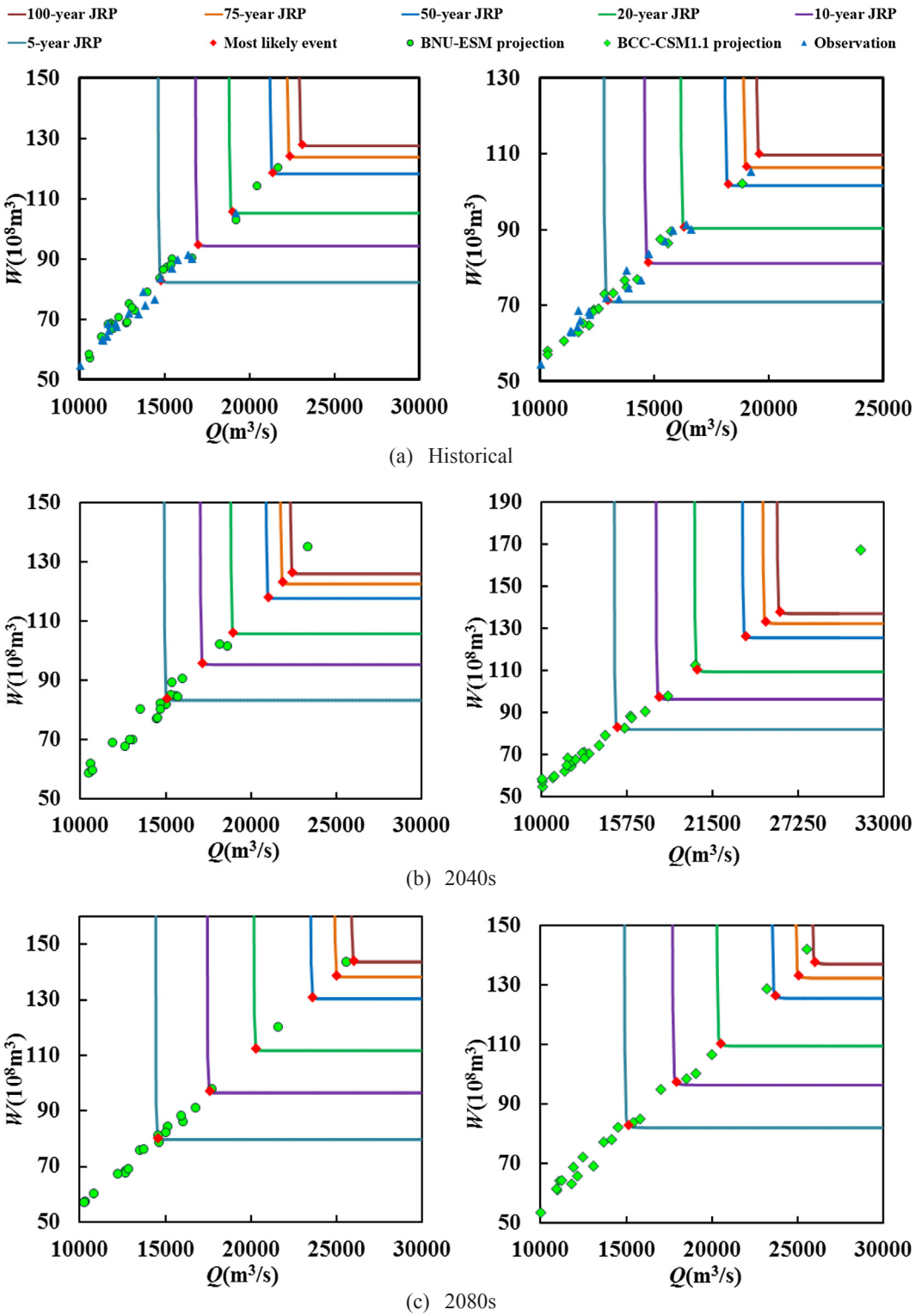

Fig. 11. Bivariate quantile for historical and future periods under two GCMs.

4. Results and discussions

4.1. Projected changes to precipitation, temperature and discharge

To detect the long-term variation of climate data in the Ganjiang River basin, the nonparametric Mann-Kendall (M-K) method is employed to examine the trends in the climate data and selected EPIs series during 1966–2099. Fig. 9 shows the Z_{MK} statistics for different climate variables and indices, and the x-axis represents the 13 variables or indices following the order in Table 3. Fig. 9 indicates a significant increasing trend of bias-corrected annual mean precipitation under BCC-CSM1.1, while the increasing trend of BNU-ESM is not significant at 5% significance level. Fig. 9 and Table 3 indicate that a significant increase of temperature is predominant for two GCMs, with 23.9% and 21.0% increase respectively during 2080s, implying that the Ganjiang River basin is projected to become warmer in the future.

The R95p and R90N decrease by 3.4% and 2.8% respectively and subsequently increase during 2080s under BNU-ESM outputs. The

Table 8
Comparison of bivariate flood quantiles changes between historical and future periods (Unit: Q, m^3/s; W, $10^8 m^3$).

Estimation period	GCM	Variable	Return Period (year)					
			100	75	50	20	10	5
Observation		*Q*	22887(22768)	22281(22296)	21403(21706)	19293(20086)	17532(18392)	15541(16582)
		W	120.6(121.9)	117.1(111.5)	112.1(110.8)	100.0(102.4)	90.0(93.8)	78.8(82.5)
Historical	BNU-ESM	*Q*	23083(22302)	22385(22856)	21377(22125)	18981(19965)	17013(17602)	14826(15264)
		W	128.0(130.5)	124.2(128.3)	118.7(123.4)	105.7(112.0)	94.9(99.2)	82.8(86.2)
	BCC-CSM1.1	*Q*	19584(20025)	19026(19010)	18222(18450)	16303(16602)	14722(15105)	12959(13520)
		W	110.0(113.6)	106.7(104.6)	102.0(101.3)	90.7(92.8)	81.5(84.2)	71.4(74.2)
2040s	BNU-ESM	*Q*	22449(24051)	21878(23410)	21043(22204)	18997(19402)	17198(17562)	15099(15540)
		Variation (%)	−2.7(3.2)	−2.3(2.4)	−1.6(0.4)	0.1(−2.8)	1.1(−0.2)	1.8(1.8)
		W	126.3(139.0)	122.9(135.1)	118.0(127.2)	106.0(108.9)	95.8(97.3)	83.7(85.9)
		Variation (%)	−1.4(6.5)	−1.0(5.3)	−0.6(3.1)	0.4(−2.8)	1.0(−1.9)	1.2(−0.3)
	BCC-CSM1.1	*Q*	26069(32000)	25114(31400)	23746(30520)	20536(19780)	17953(17245)	15154(14705)
		Variation (%)	33.1(59.8)	32.0(65.2)	30.3(65.4)	26.0(19.1)	21.9(14.2)	16.9(8.8)
		W	137.7(170.3)	133.0(166.0)	126.2(160.6)	110.2(107.2)	97.1(92.8)	82.8(79.7)
		Variation (%)	25.2(49.9)	24.6(58.7)	23.8(58.5)	21.4(15.5)	19.1(10.2)	16.0(7.4)
2080s	BNU-ESM	*Q*	26034(26920)	25063(26105)	23665(24820)	20346(20985)	17627(18253)	14960(15460)
		Variation (%)	12.8(15.5)	12.0(14.2)	10.7(12.2)	7.2(5.1)	3.6(3.7)	0.9(1.3)
		W	144.0(151.2)	138.6(146.2)	130.7(138.3)	112.1(116.2)	96.9(99.7)	83.8(86.8)
		Variation (%)	12.5(15.9)	11.6(14.0)	10.1(12.1)	6.1(3.8)	2.2(0.5)	1.2(0.7)
	BCC-CSM1.1	*Q*	27906(33012)	26785(32105)	23895(25062)	21536(22106)	18356(19026)	15215(15603)
		Variation (%)	42.5(64.9)	40.8(68.9)	31.1(35.8)	32.1(33.2)	24.7(26.0)	17.4(15.4)
		W	151.7(178.3)	145.3(168.9)	131.2(132.6)	117.1(121.2)	101.3(103.6)	87.6(85.9)
		Variation (%)	37.9(57.0)	36.1(61.5)	34.6(30.1)	29.1(30.6)	24.2(23.0)	22.7(15.8)

changes of the R95p and R90N indices represent extreme precipitation percentiles, showing a consistent significant increase under BCC-CSM1.1. This may imply that the magnitude of extreme precipitation tends to increase under RCP 8.5 scenario. As an indicator of flood-producing events, the future Rx5day under BCC-CSM1.1 increases gradually while BNU-ESM projects an increase until the end of 21st century after a 1.3% decrease during 2040s, which pose a threat to the safety of flood control in this basin. A general increase of SDII is projected under two GCMs, except for a slight decrease of 0.9% during 2040s under BNU-ESM. Overall, there is a trend of centralized precipitation in this basin under RCP8.5. CDD and CWD indicate extreme precipitation persistence, with CDD relating to drought and CWD relating to flood. Projected significant increase of CDD in the future ranges from 11.4%–32.7% and 13.7%–22.0% for BNU-ESM and BCC-CSM1.1 respectively, indicating increasing risks of consecutive dry days, which is consistent with the decreasing trend of streamflow in dry seasons, i.e. autumn (September, October and November) and winter (December, January, and February). Meanwhile, CWD is projected to slightly decrease in the 2040s and then significantly increase by 14.7% in the latter 21st century under BNU-ESM, while a consistent increasing trend of CWD is found under BCC-CSM1.1. This may imply that the Ganjiang River basin will probably experience more sudden changes from droughts to floods in the future under RCP8.5. Projected changes in annual and seasonal mean streamflow during future periods (2040s and 2080s) in the Ganjiang River basin are illustrated in Table 3, showing that the streamflow will be concentrated during spring and summer under two GCMs, which is the same as observation series. Table 3 also projects a general increasing trend of streamflow in annual, spring and summer scales. These projections are consistent with meteorological change, while the increasing annual temperature, precipitation, magnitude indices (R95p, R90N) and intensity indices (Rx5day, SDII) both projects a general moister and warmer climate in the future.

4.2. Fitting marginal and joint distributions

The annual maximum (AM) sampling method was used to obtain the annual maximum flood peak (Q) and annual maximum 7-day flood volume (W) for the historical and future flood scenarios respectively. It is noted that the volume associated with the peak discharge are definitely annual maximums, which might be independent of the peak flow event (Xu et al., 2016).

Table 4 demonstrates root mean square error (RMSE), Akaike information criterion (AIC) and Kolmogorov-Smirnov (K-S) statistic D_{ks} for parametric and nonparametric estimation methods. It is evident that all the distributions can pass the K-S test because $D_{ks} < D_{0.05}$; however, the P-III distribution shows good performance than other distributions in most cases while Gamma distribution and nonparametric methods perform better in two cases. To ease the implementation of comparing climate change on flood quantiles, only the optimal parametric and nonparametric methods are employed to estimate flood quantiles for different periods. The frequency curves shown in Fig. 10 reveal that the nonparametric method is not sensitive to data type and could be effectively used for a well estimate of the floods, for example during 2040s period, the parametric method fails to capture the outlier flood data (extreme wet year in 2056) of BCC-CSM1.1 while the nonparametric approach estimation is very close to the data series. However, the nonparametric approach does not have a theoretical distribution and may have certain limitations for extrapolating, especially when the sample size is small.

The Pearson, Kendall and Spearman correlation coefficients were calculated to assess the dependence between Q and W for observation, historical and future periods, and their estimated values are listed in Table 5. It is shown that the mutually correlated nature of Q and W for observed and projected scenarios is clearly visible, which supports the necessity for bivariate flood frequency analysis. The copula parameter and statistical test results are listed in Table 6, which indicates that the G-H copula has the smallest RMSE, AIC and D_{ks} values. Hence, the G-H copula is selected for modeling the dependence between the Q and W for both the historical and future periods.

4.3. Univariate analysis of historical and projected scenarios

For different return periods (T = 100, 75, 50, 20, 10, 5-year), the corresponding quantiles of Q and W for observation, historical and projected scenarios are estimated based on the optimal parametric and nonparametric methods and listed in Table 7. It can be noticed from Table 7 that two GCMs simulates extreme floods well during the

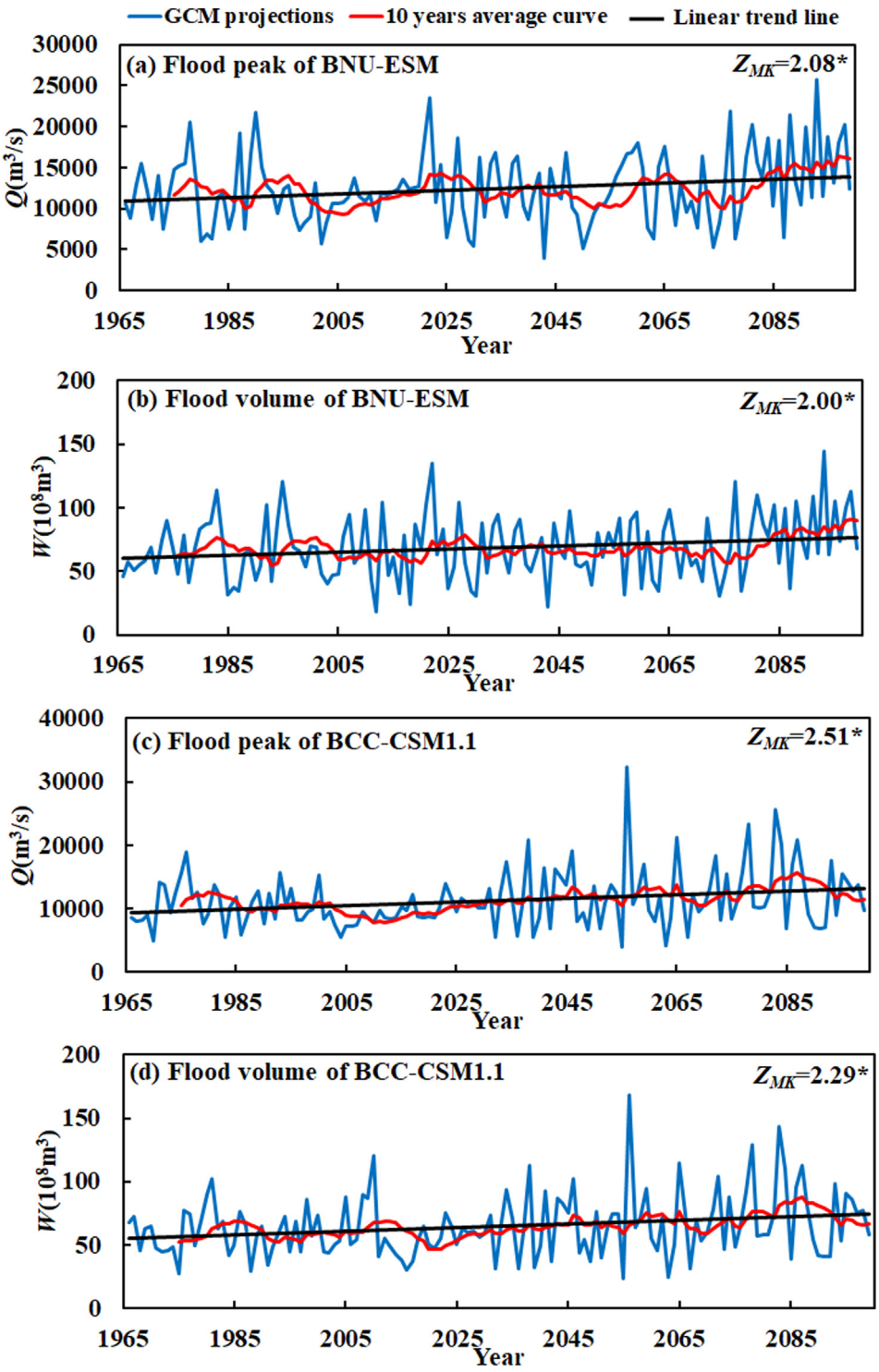

Fig. 12. Mann–Kendall trend test of flood peak and volume series during 1965–2099 under two GCMs.

historical period. The differences between the parametric and nonparametric methods are not as large as two different GCMs. From Table 7, parametric and nonparametric methods yield the similar conclusion, i.e. there are increasing tendency toward changes for projections of future flood characteristics except a little decrease occurred in 2040s for BNU-ESM. During 2080s, two GCMs project that *Q* and *W* increase by 12.1%–42.4% and 11.6%–37.4% under return periods higher than 50-year, respectively. This might be a signal of changes in the climate for that area toward moister climate based on the BNU-ESM and BCC-CSM1.1 under RCP 8.5 scenario. Table 7 also indicates that the variability increases with the return period, and the *Q* have larger increments than *W*. These may imply that the climate change has heavier impacts on *Q* than *W* and larger flood events are likely to happen in future for Ganjiang River basin under RCP 8.5 scenario.

4.4. Bivariate analysis of historical and projected scenarios

Fig. 11 demonstrates the bivariate quantile curves for historical and future periods under the selected G-H copula. The observations and GCMs projected flood events are also shown in Fig. 11 in order to obtain

Table 9
Summary of estimated parameters of the optimal non-stationary marginal and copula functions.

GCM	Variable	Optimal distribution	μ^t	σ^t	κ	θ_c^t	RMSE	AIC	D_{ks}
BNU-ESM	Q	P-III	$9.1056 + 0.0019 \times Prep^t$	$-1.1282 + 0.0028 \times Prep^t$	0.37		0.035	−262.2	0.065
	W	P-III	$3.6827 + 0.0017 \times Prep^t$	$-1.3702 + 0.0034 \times Prep^t$	0.38		0.031	−271.9	0.052
	Q-W	G-H				$1.2105 + 0.0014 \times Prep^t$	0.015	−334.0	0.014
BCC-CSM1.1	Q	P-III	$9.3015 + 0.0021 \times Prep^t$	$-0.8808 + 0.0018 \times Prep^t$	1.10		0.038	−255.6	0.067
	W	P-III	$4.0927 + 0.0015 \times Prep^t$	$-0.8898 + 0.0021 \times Prep^t$	1.04		0.034	−264.5	0.058
	Q-W	G-H				$1.2314 + 0.0016 \times Prep^t$	0.019	−315.1	0.016

$Prep^t$ indicates the annual total precipitation at the t^{th} year.

a rough estimation of their magnitude in the bivariate context. For the historical and 2080s periods, the largest flood events are located below the $T_{or} = 100$ year curve, while one outlier flood projection over $T_{or} = 100$ year curve happened for both two GCMs during 2040s. The most likely design realization method is used to estimate Q and W joint quantiles, and the estimation results are presented in Table 8. Similar to the univariate analysis, the differences of observation and historical floods are not so noticeable, and the estimation differences between parametric and nonparametric method is lower than those of different GCMs.

Comparing the estimated quantiles in Tables 7 and 8, it is found that the univariate estimators are smaller than the bivariate ones. This is due to the fact that the conventional univariate methods usually lead to underestimation (for OR JRP) or over estimation (for AND JRP). Fig. 11 and Table 8 show that there is an obvious increase for the higher return periods. For example, the parametric analysis indicate that the Q and W increase by 12.5%–42.5% under 100-year JRP during 2080s, while increase by 0.9%∼22.7% under 5-year JRP. These results imply that the joint quantile corresponding to larger return periods will be affected more by climate change than those corresponding to small return periods under BNU-ESM and BCC-CSM1.1, which the change may increase future flood risks in Ganjiang River basin. The change to floods is consistent with the general increasing trend of magnitude indices (R95p and R90N) and intensity indices (Rx5day and SDII) analyzed in Section 4.1.

4.5. Adaptive bivariate flood quantile estimation

The Q and W series during 1965–2099 are plotted in Fig. 12, and results of the M-K trend test are denoted on each plot. Significant increasing trends are detected by the M-K test for two GCMs at 5% significance level. The nonparametric Pettitt test (Pettitt, 1979) is applied to investigate the presence of abrupt changes for both Q and W. According to the results of the Pettitt test, the Q and W under BCC-CSM1.1 both present a significant abrupt change in 2022, and the BNU-ESM GCM show a significant abrupt change in 2070. These preliminary analyses just demonstrate that both Q and W under two GCMs are non-stationary, which supports the necessity of non-stationary analysis for the merged series under climate change. The non-stationary marginal and copula functions are fitted using time-varying moment method under the GAMLSS framework. To find the best-fit non-stationary model, three precipitation variables ($Prep$, $Prep^{SP}$ and $Prep^{SU}$) as well as time are selected as candidate explanatory variables while temperature is excluded as it has little correlation with flood. In this study, three two-parameter distributions, i.e., Lognormal, Gamma and Gumbel, and two three-parameter distributions, i.e. GEV and P-III, that widely used in modelling flood data are considered as candidates. Considering that the shape parameter κ of P-III and GEV distributions is quite sensitive, we assumed it to be constant as other studies did (e.g. Leclerc and Ouarda, 2007; Bender et al., 2014; Um et al., 2017). For the ease of parameter estimation and avoiding over-parameterization, three Archimedean copulas, i.e. G-H, Frank and Clayton copula are selected as the candidates in modeling the time-varying dependence between flood peak and volume. The non-stationary models with the smallest AIC values are selected and demonstrated in Table 9, which shows that the $Prep$ is the best explanatory for all the variables.

In this study we focus exemplarily on events with a 50-year JRP, because in general events with lower JRPs are of interests for hydrological engineering practice and have small uncertainties of extrapolation (Bender et al., 2014). Fig. 13 shows the evolution of the ensemble of isolines under 50-year JRP during 1966–2099. For the sake of comparison, the 50-year isolines derived from the merged series during 1965–2099 using stationary method are also given in Fig. 13, which reveals that the isolines cross each other and cover a broad range, for example, under BNU-ESM, the 50-year isolines covering a range with marginal Q and W values ranging from 19157 m^3/s to 27495 m^3/s and $96 \times 10^8 m^3$ to $165 \times 10^8 m^3$, respectively. It is also shown that there is one high outlier isoline for BCC-CSM1.1 GCM; this is due to the fact that an outlier large flood occurs in the extreme wet year (2056) as shown in Fig. 13.

Next, we focus on the development of the most likely events where the joint probability densities have their maximum values on each isoline derived by solving Eq. (17). Fig. 14 illustrates the time

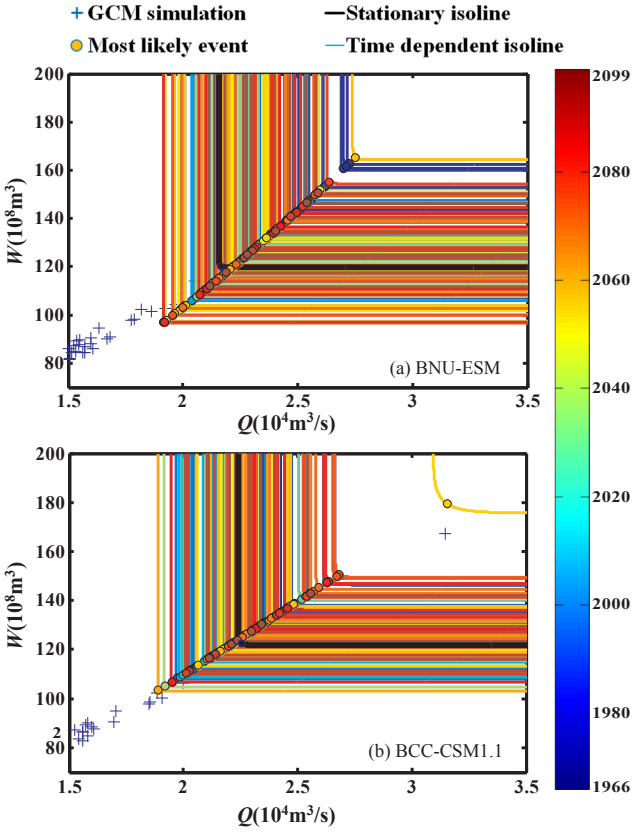

Fig. 13. Time dependent probability-isolines under 50-year JRP for the non-stationary data series derived by two GCMs.

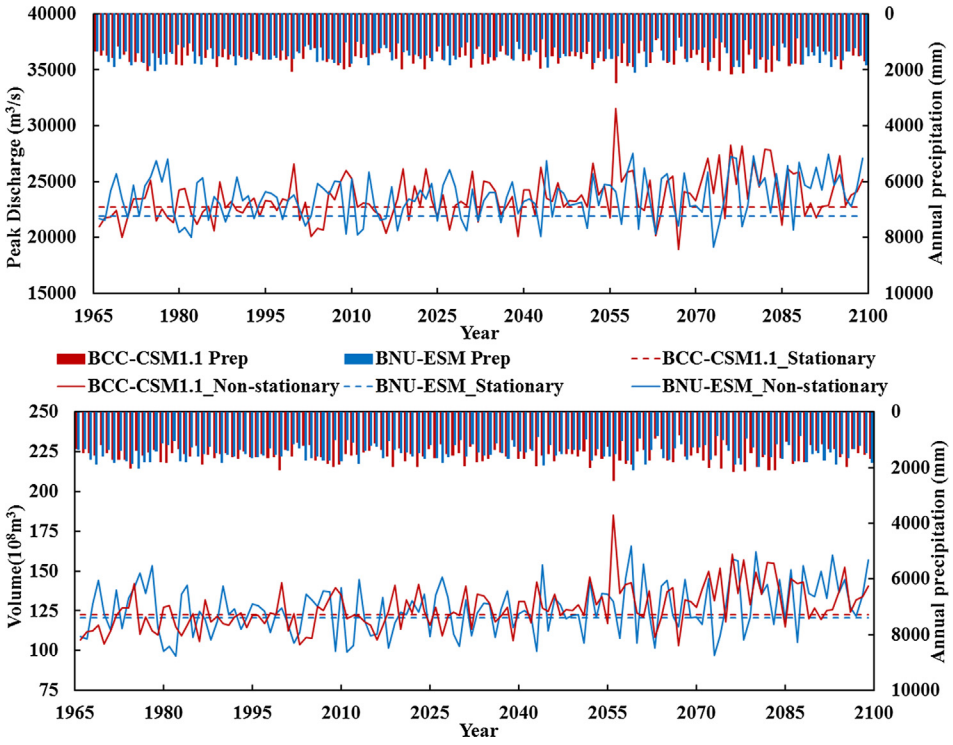

Fig. 14. Time dependent development of the most likely flood quantiles of *Q* and *W* under 50-year JRP derived by non-stationary models.

Table 10
Average adaptive bivariate flood quantiles and the relative difference with stationary estimations during historical and future periods under 50-year JRP (Unit: *Q*, m^3/s; *W*, $10^8 m^3$).

GCM		Historical		2040s		2080s	
		Q	*W*	*Q*	*W*	*Q*	*W*
BNU-ESM	Value	23,319	123.1	23,523	125.9	24,363	133.6
	RD (%)	9.08	3.71	11.79	6.69	2.95	2.22
BCC-CSM1.1	Value	21,985	117.6	23,968	128.7	24,652	134.8
	RD (%)	20.65	15.29	0.93	1.98	3.17	2.74

dependent development of both *Q* and *W*, showing that the larger floods occurred when the annual total precipitation (*Prep*) is heavier. This is reasonable due to the explanatory variables for the optimal non-stationary models are chosen as *Prep*. Figs. 13 and 14 both show that the joint probability and flood quantile vary significantly over time when non-stationary models are applied. Fig. 14 indicates that the values of quantile *Q* range from 21690 m^3/s in 1966 to 27104 m^3/s in 2099 (or 25.0% increase) under BNU-ESM, and the largest flood 27496 m^3/s occurs in extreme wet year of 2059. The flood peak quantile has wider range under BCC-CSM1.1 than that of BNU-ESM, and the *Q* range from 18580 m^3/s to 31550 m^3/s. The changes to flood are consistent to the increasing trend of *Prep*; for example, *Prep* increases from 1338 mm in 1966 to 1775 mm in 2099 by 32.7% under BNU-ESM. To compare the projected changes by the non-stationary method, Table 10 lists the average adaptive bivariate flood quantiles and the relative difference (RD) with stationary estimations during historical and future periods under 50-year JRP. The two GCMs both show a positive trend and that in most years the design flood peaks are far larger than the stationary estimations. The temporal evolution of the design values of *W* is similar as described for *Q*. These findings imply that climate change have large impacts on the future flood characteristics under RCP 8.5 scenario and large uncertainty and risks of the flood hazard should be taken into considerations for future engineering design.

5. Conclusions

Climate change is expected to have an effect on future storm characteristics, and the change should properly be taken into account when evaluating future flood characteristics. This study evaluated the flood quantiles of peak discharge and volume for the current (1966–2005) and future (2020–2099) periods in the Ganjiang River basin using univariate and copula-based bivariate frequency analysis methods. The mutually correlated nature of flood peak and volumes visible clearly in the simulated flood events under both BNU-ESM and BCC-CSM1.1 GCMs supports the necessity for bivariate flood frequency analysis. The adaptive flood quantiles under 50-year JRP were derived using the non-stationary most likely event selection method by employing time-varying moment method. The main results are summarized as follows.

(1) From univariate analysis of historical and RCP 8.5 projected scenarios, two GCMs both indicate that a signal of changes in the climate for the Ganjiang River basin toward moister climate under the 8.5 scenario. During 2080s, two GCMs projects that the flood peak and 7-day flood volume increase by 12.1%～42.4% and 11.6%～37.4% under return periods higher than 50-year, respectively.
(2) In case of bivariate analysis, there is a considerable increase for the higher return periods for the RCP 8.5 scenario. For the period 2080s, the flood peak and 7-day flood volume increase by 12.5%～42.5% under 100-year JRP, while increase by 0.9%～22.7% under 5-year JRP. It is shown that the joint quantiles corresponding to larger return periods will be affected more by climate change than those corresponding to small return periods under two GCMs.
(3) The adaptive isolines and most likely events under 50-year JRP are derived from analyzing the merged series by non-stationary copula-based models. The results reveal that the isolines cross each other and cover a broad range. Climate change has considerable impacts on the future bivariate flood quantiles, and thus the resulting uncertainty and risks of the flood hazard should be taken into consideration for engineering design and water resources management.

In general, the above findings have highlighted the importance of considering the climate change and non-stationary in the bivariate flood quantile estimation. However, only two GCMs and one statistical downscaling method have been employed to project future streamflow. Since the impact of climate change on floods is the comprehensive outcome, we should take consideration of the uncertainty of GCMs and downscaling methods in the future work. Also, this study only focuses on bivariate framework; multivariate analysis of flood peak, volume and duration considering integrated uncertainties under climate change needs further research.

Acknowledgements

This study is financially supported by the National Key Research and Development Plan of China (Grant NO. 2016YFC0402206) and the National Natural Science Foundation of China (Grant NO. 51539009, 51579183). We are very grateful to the editor and anonymous reviewers for their valuable comments and constructive suggestions that helped us to greatly improve the manuscript. The authors also would like to acknowledge the contribution of the World Climate Research Program Working Group on Coupled Modelling, and to thank climate modeling groups for making available their respective climate model outputs.

References

Adamowski, K., 1985. Nonparametric kernel estimation of flood frequencies. Water Resour. Res. 21 (11), 1885–1980.
Ahmadalipour, A., Moradkhani, H., Rana, A., 2018. Accounting for downscaling and model uncertainty in fine-resolution seasonal climate projections over the columbia river basin. Clim. Dyn. 50, 717–733.
Booij, M.J., 2005. Impact of climate change on river flooding assessed with different spatial model resolutions. J. Hydrol. 303 (1), 176–198.
Bowman, A., Azzalini, A., 1997. Applied Smoothing Techniques for Data Analysis: The Kernel Approach with S-plus Illustrations. Oxford University Press, New York.
Bender, J., Wahl, T., Jensen, J., 2014. Multivariate design in the presence of non-stationarity. J. Hydrol. 514, 123–130.
Chen, J., Brissette, F.P., Leconte, R., 2011. Uncertainty of downscaling method in quantifying the impact of climate change on hydrology. J. Hydrol. 401 (3), 190–202.
Chen, J., Brissette, F.P., Chaumont, D., Braun, M., 2013a. Performance and uncertainty evaluation of empirical downscaling methods in quantifying the climate change impacts on hydrology over two North American river basins. J. Hydrol. 479, 200–214.
Chen, J., Brissette, F.P., Chaumont, D., Braun, M., 2013b. Finding appropriate bias correction methods in downscaling precipitation for hydrologic impact studies over north america. Water Resour. Res. 49 (7), 4187–4205.
Chen, L., Singh, V.P., 2018. Entropy-based derivation of generalized distributions for hydrometeorological frequency analysis. J. Hydrol. 557, 699–712.
Chebana, F., Ouarda, T.B., 2011. Multivariate quantiles in hydrological frequency analysis. Environmetrics 22 (1), 63–78.
Das, T., Dettinger, M.D., Cayan, D.R., Hidalgo, H.G., 2011. Potential increase in floods in Californian Sierra Nevada under future climate projections. Clim. Change 109 (1), 71–94.
De Michele, C., Salvadori, G., Canossi, M., Petaccia, A., Rosso, R., 2005. Bivariate statistical approach to check adequacy of dam spillway. J. Hydrol. Eng. 10, 50–57.
De Michele, C., Salvadori, G., Vezzoli, R., Pecora, S., 2013. Multivariate assessment of droughts: frequency analysis and dynamic return period. Water Resour. Res. 49, 6985–6994.
Duan, K., Mei, Yadong, Zhang, L., 2016. Copula-based bivariate flood frequency analysis in a changing climate – a case study in the Huai River basin. China. J. Earth Sci. 27, 37–46.
Durman, C.F., Gregory, J.M., Hassel, D.C., Jones, R.G., Merphy, J.M., 2001. A comparison of extreme European daily precipitation simulated by a global and a regional climate model for present and future climates. Q. J. R. Meteorol. Soc. 127, 1005–1015.
Favre, A.C., El Adlouni, S., Perreault, L., Thiémonge, N., Bobée, B., 2004. Multivariate hydrological frequency analysis using copulas. Water Resour. Res. 40 (1), W01101. https://doi.org/10.1029/2003WR002456.
Greenwood, J.A., Landwehr, J.M., Matalas, N.C., Wallis, J.R., 1979. Probability weighted moments: definition and relation to parameters of several distributions expressable in inverse form. Water Resour. Res. 15 (5), 1049–1054.
Guo, S., Kachroo, R.K., 1996. Nonparametric estimation with low flood data. J Hydrol. 185 (1–4), 335–348.
Hosking, J.R.M., 1990. L-moments: analysis and estimation of distributions using linear combinations of order statistics. J. Roy. Stat. Soc. Ser. B 52, 105–124.
Hu, Q., Feng, S., Guo, H., Chen, G., Jiang, T., 2007. Interactions of the Yangtze river flow and hydrologic processes of the Poyang Lake. China. J. Hydrol. 347 (1), 90–100.
Huziy, O., Sushama, L., Khaliq, M.N., Laprise, R., Lehner, B., Roy, R., 2013. Analysis of streamflow characteristics over Northeastern Canada in a changing climate. Clim. Dynam. 40 (7–8), 1879–1901.
IPCC., 2014. Climate change 2014: Impacts Adaptation and Vulnerability and Climate Change 2014: Mitigation of Climate Change. Contribution of working group II and working group III to the fifth assessment report of the IPCC. Cambridge University Press, New York.
Jeong, D.I., Sushama, L., Khaliq, M.N., Roy, R., 2014. A copula-based multivariate analysis of Canadian RCM projected changes to flood characteristics for northeastern Canada. Clim. Dynam. 42 (7–8), 2045–2066.
Ji, D., Wang, L., Feng, J., Wu, Q., Cheng, H., 2014. Basic evaluation of beijing normal university earth system model (BNU-ESM) version 1. Geosci. Model Dev. 7 (5), 2039–2064.
Joe, H., 2005. Asymptotic efficiency of the two-stage estimation method for copula-based models. J. Multivariate Anal. 94 (2), 401–419.
Leclerc, M., Ouarda, T.B.M.J., 2007. Non-stationary regional flood frequency analysis at ungauged sites. J. Hydrol. 343, 254–265.
Lin, K., Lv, F., Chen, L., Singh, V.P., Zhang, Q., Chen, X., 2014. Xinanjiang model combined with curve number to simulate the effect of land use change on environmental flow. J. Hydrol. 519, 3142–3152.
Ma, C., Pan, S., Wang, G., Liao, Y., Xu, Y.P., 2016. Changes in precipitation and temperature in xiangjiang river basin, china. Theor. Appl. Climatol. 123 (3), 1–13.
Mann, H.B., 1945. Nonparametric tests against trend. Econometrica 13 (3), 245–259. http://www.jstor.org/stable/1907187.
Meaurio, M., Zabaleta, A., Boithias, L., et al., 2017. Assessing the hydrological response from an ensemble of cmip5 climate projections in the transition zone of the atlantic region (bay of biscay). J. Hydrol. 548, 46–62.
Mpelasoka, F.S., Chiew, F.H.S., 2009. Influence of rainfall scenario construction methods on runoff projections. J. Hydrometeorol. 10, 1168–1183.
Nelsen, R.B., 1999. An Introduction to Copulas. Springer, New York.
Nelsen, R.B., 2006. An Introduction to Copulas, 2nd Edition. Springer-Verlag, New York.
Özban, A., 2004. Some new variants of Newton's method. Appl. Math Lett. 17 (6), 677–682.
Pettitt, A.N., 1979. A non-parametric approach to the change-point problem. J. Appl. Stat. 28, 126–135.
Poulin, A., Huard, D., Farve, A., Pugin, S., 2007. Importance of tail dependence in bivariate frequency analysis. J. Hydraul. Eng. 12 (4), 394–403.
Prudhomme, C., Reynard, N., Crooks, S., 2002. Downscaling of global climate models for flood frequency analysis: where are we now? Hydrol. Process 16 (6), 1137–1150.
Requena, A.I., Chebana, F., Mediero, L., 2016. A complete procedure for multivariate index-flood model application. J. Hydrol. 535, 559–580.
Rigby, R.A., Stasinopoulos, D.M., 2005. Generalized additive models for location, scale and shape. J. Roy. Stat. Soc. C – Appl. Stat. 54 (3), 507–554.
Rosenbrock, H.H., 1960. An automatic method for finding the greatest or least value of a function. Comput. J. 3 (3), 175–184.
Salvadori, G., De Michele, C., 2004. Frequency analysis via copulas: theoretical aspects and applications to hydrological events. Water Resour. Res. 40 (12).
Salvadori, G., De Michele, C., Durante, F., 2011. On the return period and design in a multivariate framework. Hydrol. Earth Syst. Sci. 15, 3293–3305.
Salvadori, G., Durante, F., De Michele, C., Bernardi, M., Petrella, L., 2016. A multivariate Copula-based framework for dealing with Hazard Scenarios and Failure Probabilities. Water Resour. Res. 52 (5), 3701–3721.
Schmidli, J., Frei, C., Vidale, P.L., 2006. Downscaling from GCM precipitation: a benchmark for dynamical and statistical downscaling methods. Int. J. Climatol. 26, 679–689.
Scott, D.W., 1992. Multivariate Density Estimation: Theory. Practice and Visualization, Wiley, New York.
Shen, M., Chen, J., Zhuan, M., Chen, H., Xu, C.-Y., Xiong, L., 2018. Estimating uncertainty and its temporal variation related to global climate models in quantifying climate change impacts on hydrology. J. Hydrol. 556, 10–24.
Shiau, J.T., 2003. Return period of bivariate distributed extreme hydrological events. Stoch. Env. Res. Risk Assess. 17 (1), 42–57.
Silverman, B.W., 1986. Density Estimation for Statistics and Data Analysis. Published in Momographs on Statistics and Applied Probability, Chapman and Hall, London.
Sklar, A., 1959. Fonctions de répartition à n dimensions et leurs marges. Publications de l'Institut de Statistique de L'UniversitéParis 8, 229–231.
Swansburg, E., El-Jabi, N., Caissie, D., 2004. Climate change in New Brunswick (Canada): statistical downscaling of local temperature, precipitation, and river discharge, Canada. Tech. Rep. Fish. Aquat. Sci. 2544, 42p.
Taylor, K.E., Stouffer, R.J., Meehl, G.A., 2012. An overview of CMIP5 and the experiment design. Bull. Amer. Meteor. Soc. 93 (4), 485–498.
Teng, J., Vaze, J., Chiew, F.H.S., Wang, B., Perraud, J.M., 2012. Estimating the relative uncertainties sourced from GCMs and hydrological models in modeling climate change impact on runoff. J. Hydrometeorol. 13 (1), 122–139.
Themeßl, M.J., Gobiet, A., Leuprecht, A., 2010. Empirical statistical downscaling and error correction of daily precipitation from regional climate models. Int. J. Climatol http://dx.doi.org/10.1002.joc.2168.
Tofiq, F.A., Guven, A., 2014. Prediction of design flood Discharge by statistical downscaling and General Circulation Models. J. Hydrol. 517, 1145–1153.
Tofiq, F.A., Guven, A., 2015. Potential changes in inflow design flood under future climate projections for Darbandikhan Dam. J. Hydrol. 528, 45–51.
Um, M.-J., Kim, Y., Markus, M., Wuebbles, D.J., 2017. Modeling nonstationary extreme value distributions with nonlinear functions: an application using multiple precipitation projections for U.S. cities. J. Hydrol. 552, 396–406.
Vittal, H., Singh, J., Kumar, P., Karmakar, S., 2015. A framework for multivariate data-based at-site flood frequency analysis: essentiality of the conjugal application of parametric and nonparametric approaches. J. Hydrol. 525, 658–675.
Volpi, E., Fiori, A., 2012. Design event selection in bivariate hydrological frequency

analysis. Hydrol. Sci. J. 57 (8), 1506–1515.
Volpi, E., Fiori, A., 2014. Hydraulic structures subject to bivariate hydrological loads: Return period, design, and risk assessment. Water Resour. Res. 50, 885–897.
Wang, L., Guo, S., Hong, X., Xiong, L., 2016. Projected hydrologic regime changes in the Poyang Lake Basin due to climate change. Front. Earth Sci. 2016, 1–19.
Wilby, R.L., Dawson, C.W., Barrow, E.M., 2002. SDSM-a decision support tool for the assessment of regional climate change impacts. Environ. Modell. Softw. 17 (2), 147–159.
Xin, X., Wu, T., Li, J., Wang, Z., Li, W., Wu, F., 2013. How well does BCC_CSM1. 1 reproduce the 20th century climate change over China? Atmospheric and Oceanic. Science Letters 6 (1), 21–26.
Xu, C.-Y., 1999. From GCMs to river flow: a review of downscaling methods and hydrologic modelling approaches. Prog. Phys. Geogr. 23, 229–249.
Xu, C., Yin, J., Guo, S., Liu, Z., Hong, X., 2016. Deriving design flood hydrograph based on conditional distribution: a case study of danjiangkou reservoir in hanjiang basin. Math Probl. Eng. https://doi.org/10.1155/2016/4319646.
Xu, C.-Y., Singh, V.P., 2001. Evaluation and generalization of temperature-based methods for calculating evaporation. Hydrol. Processes 15 (2), 305–319.
Yin, J., Guo, S., Liu, Z., Chen, K., Chang, F.J., Xiong, F., 2017. Bivariate seasonal design flood estimation based on copulas. J. Hydrol. Eng. 22 (12), 05017028. https://doi.org/10.1061/(ASCE)HE.1943-5584.0001594.
Yin, J., Guo, S., Liu, Z., Yang, G., Zhong, Y., Liu, D., 2018. Uncertainty analysis of bivariate design flood estimation and its impacts on reservoir routing. Water Resour. Manag. 32 (5), 1795–1809.
Zhao, R.J., Zhang, Y.L., Fang, L.R., Liu, X.R., Zhang, Q.S., 1980. The Xinangjiang model. Proc., Oxford Symposium on Hydrological Forecasting. Int. Association of Hydrological Sciences, Wallingford, U.K. 351–356.
Zhao, R.J., 1992. The Xinanjiang model applied in China. J. Hydrol. 135 (1), 371–381.
Zhang, L., Singh, V.P., 2006. Bivariate flood frequency analysis using the copula method. J. Hydrol. Eng. 11 (2), 150–164.
Zhang, W., Liu, P., Wang, H., Chen, J., Lei, X., Feng, M., 2017. Reservoir adaptive operating rules based on both of historical streamflow and future projections. J. Hydrol. 553, 691–707.
Zhuan, M., Chen, J., Shen, M., Xu, C.-Y., Chen, H., Xiong, L., 2018. Timing of human-induced climate change emergence from internal climate variability for hydrological impact studies. Hydrol. Res. https://doi.org/10.2166/nh. 2018.059.